Neuroscience

Serotonergic and dopaminergic neurons in the dorsal raphe are differentially altered in a mouse model for parkinsonism

Laura Boi, Yvonne Johansson, Raffaella Tonini, Rosario Moratalla, Gilberto Fisone, Gilad Silberberg

Department of Neuroscience, Karolinska Institutet, Stockholm 17177, Sweden • Sainsbury Wellcome Centre for Neural Circuits and Behaviour, University College London, London, UK • Neuromodulation of Cortical and Subcortical Circuits Laboratory, Istituto Italiano di Tecnologia, Genova, Italy • Cajal Institute, Spanish National Research Council (CSIC), Madrid, Spain • CIBERNED, Instituto de Salud Carlos III, Madrid, Spain

Reviewed Preprint

Revised by authors after peer review.

About eLife's process

Reviewed preprint version 2
April 4, 2024 (this version)

Reviewed preprint version 1
August 21, 2023

Posted to preprint server
July 22, 2023

Sent for peer review
July 5, 2023

Abstract

Parkinson's disease (PD) is characterized by motor impairments caused by degeneration of dopamine neurons in the substantia nigra pars compacta. In addition to these symptoms, PD patients often suffer from non-motor co-morbidities including sleep and psychiatric disturbances, which are thought to depend on concomitant alterations of serotonergic and noradrenergic transmission. A primary locus of serotonergic neurons is the dorsal raphe nucleus (DRN), providing brain-wide serotonergic input. Here, we identified electrophysiological and morphological parameters to classify serotonergic and dopaminergic neurons in the murine DRN under control conditions and in a PD model, following striatal injection of the catecholamine toxin, 6-hydroxydopamine (6-OHDA). Electrical and morphological properties of both neuronal populations were altered by 6-OHDA. In serotonergic neurons, most changes were reversed when 6-OHDA was injected in combination with desipramine, a noradrenaline reuptake inhibitor, protecting the noradrenergic terminals. Our results show that the depletion of both noradrenaline and dopamine in the 6-OHDA mouse model causes changes in the DRN neural circuitry.

eLife assessment

This **important** work provides a **convincing** dataset of neuronal heterogeneity in the raphe nucleus, including their physiological properties, morphology, and susceptibility to the neurodegeneration of noradrenaline and dopamine systems in the Parkinsonian state. These findings suggest a significant interplay between catecholaminergic systems in healthy and parkinsonian conditions, as well as neuronal structure and function. Such findings provide a strong foundation for basic scientists as well as pre-clinical researchers interested in the role of dorsal raphe neurons in Parkinson's disease.

Introduction

Parkinson's Disease (PD) is a frequent neurodegenerative disorder characterized by the progressive loss of dopaminergic (DA) neurons in the nigrostriatal pathway, leading to bradykinesia, tremor, rigidity, and postural instability [1, 2]. These cardinal motor symptoms are typically addressed by administration of dopaminergic drugs or by deep brain stimulation. PD patients also experience non-motor symptoms including sleep, affective, and cognitive dysfunctions often preceding the motor disabilities [3, 4]. These comorbidities are in large part refractory to current PD treatments and are thought to be caused by neurodegenerative processes occurring in concomitance to the loss of midbrain dopaminergic neurons. However, the pathology underlying non-motor symptoms remains poorly understood.

Post-mortem studies in PD patients provided first insights into the brain areas which might be involved in the etiology of non-motor dysfunctions in PD. Besides the profound degeneration of the substantia nigra pars compacta (SNc), these studies found cell loss and reduced neurotransmitter release in other monoaminergic brain regions, including the dorsal and median raphe nuclei (DRN and MRN, respectively), and the locus coeruleus (LC) [1, 5–8]. The DRN constitutes the main source of serotonin in the brain with serotonergic cells ($DRN^{5\text{-}HT}$) accounting for 30-50% of its neurons [9]. $DRN^{5\text{-}HT}$ neurons have been implicated in numerous neuropsychiatric diseases, rendering them a potential neural substrate for non-motor symptoms in PD. $DRN^{5\text{-}HT}$ neurons are also of central interest in PD research because of their bidirectional, monosynaptic connection with the striatum [10, 11]. In fact, several studies have shown that serotonergic markers and transmitter levels are altered in Parkinson patients as well as in non-human primate and rodent models of PD [12–19]. Notably, alterations in the serotonergic system have also been related to non-motor comorbidities in PD [20, 21]. Yet, functional investigations of $DRN^{5\text{-}HT}$ in rodent models of PD have led to conflicting results showing both increased and decreased activity in $DRN^{5\text{-}HT}$ neurons themselves as well as in their downstream targets [22–24]. Besides the serotonergic neurons, the DRN comprises other neuronal populations, including a small group (~1000 neurons in rats) of DA neurons (DRN^{DA})[25]. DRN^{DA} neurons have been linked to the regulation of pain, motivational processes, incentive memory, wakefulness and sleep-wake transitions [26–30], but their ultimate behavioral significance is yet to be elucidated [31–35]. DRN^{DA} neurons are directly innervated by dopaminergic neurons in the midbrain and have been found to show Lewy bodies in PD patients [6, 30, 36]. Yet, the physiology and pathophysiology of DRN^{DA} neurons in PD remains elusive. The sparsity of research on DRN^{DA} neurons is likely due to the technical challenges associated with targeting this population among the diverse cell types in the DRN and adjacent structures (e.g., retrorubral field, periaqueductal grey and LC), which often co-express signature genes, hampering their molecular identification and region-specific manipulations with cre driver lines [9, 36–39].

Recently, this issue has been addressed by Pinto and colleagues who showed that DRN^{DA} neurons are most faithfully labelled in transgenic mice in which the expression of cre is linked to the DA transporter (DAT-cre) [36]. Previously, the membrane properties of DRN^{DA} neurons have only been addressed in mice in which DRN^{DA} neurons were identified based on the expression of the transcription factor Pitx3 or the enzyme tyrosine hydroxylase (TH) [37]. In Pitx3-GFP mice, about 70% of GFP-positive neurons are TH-positive (TH+) as shown by immunohistochemistry. Moreover, 40% of TH+ neurons in the DRN are not labelled in these mice, suggesting that this line targets a subpopulation of DRN^{DA} neurons [37]. The widely used TH-cre reporter line has been found to show ectopic expression of cre in non-dopaminergic neurons, probably caused by a transient developmental expression of TH [40, 41]. In addition, the TH-cre line also labels noradrenergic neurons in the neighboring LC [40], which produces most of the noradrenaline (NA) in the brain and is involved in mood control, cognition, and sleep regulation [42]. The large

overlap of functions ascribed to the LC and DRN is thought to result from the complex reciprocal synaptic connections between these two brain areas: notably, the LC provides noradrenergic input to the DRN [43, 44] while receiving input from $DRN^{5\text{-}HT}$ neurons [45–47].

Here, we used ex vivo whole-cell patch clamp recordings and morphological reconstructions to characterize the electrophysiological and morphological properties of DRN^{DA} and $DRN^{5\text{-}HT}$ neurons in wild type and DAT-tdTomato mice. Moreover, we studied the impact of catecholamine depletion on DRN^{DA} and $DRN^{5\text{-}HT}$ populations in the 6-OHDA toxin model of PD.

Results

DRN^{DA} and $DRN^{5\text{-}HT}$ neurons are electrophysiologically distinct cell-types

To investigate the electrophysiological and morphological profile of DRN^{DA} neurons and to compare it to $DRN^{5\text{-}HT}$ neurons, we performed whole-cell patch clamp recordings in coronal slices of adult wild type and DAT-cre mice crossed with tdTomato reporter mice (**Figure 1A**). All neurons were filled with neurobiotin and Alexa488 while recording. Alexa488 allowed us to take snapshots of recorded neurons at different time points, thus facilitating the topographical registration of recorded neurons to the post-hoc stained slices (Suppl. Figure 1). Using this approach, we obtained complete sets of electrophysiological and morphological data from 75 neurons in the DRN. Cells were identified as $DRN^{5\text{-}HT}$ or DRN^{DA} neurons based on tryptophan hydroxylase (TPH) or TH immunoreactivity, respectively (**Figure 1A-D**). In line with Fu et al. (2010)[38], none of the recorded neurons was positive for both TPH and TH (n = 0/412). During the recordings, we used a series of depolarizing and hyperpolarizing current steps and ramps that allowed us to characterize active and passive membrane properties in detail (**Figure 1E – G**). Based on the electrophysiological data, we first tested possible differences between TH+ neurons recorded in wild-type mice and tdTomato-positive (tdTomato+) neurons recorded in DAT-tdTomato mice. We found no differences between these two groups (n = 13 TH+ vs n = 30 tdTomato+ neurons, Suppl. Figure 2A) and neither within the subset of tdTomato+ neurons when comparing TH+ to TH- negative (TH-) neurons (n = 23 TH+ vs n = 6 TH- neurons, Suppl. Figure 2A–E). Since this small number of TH- neurons were positive for DAT and their electrophysiology indistinguishable from TH+ DRN^{DA} neurons, the data was pooled. Please note that staining of recorded neurons, i.e. immunohistochemistry on slices strained by hour-long patch-clamp recordings, is more challenging as neurons can be lost after patching (no staining data) or the staining might be ambiguous. Out of 114 tdTomato+ neurons only one cell displayed a different electrophysiological profile than all other DRN^{DA} neurons, suggesting a false-positive rate of 0.8%. That neuron was TH- and displayed profoundly distinct intrinsic properties, and was therefore excluded (Suppl. Figure 2F, G). Taken together, the electrophysiological results support the use of the DAT-tdTomato mouse line when studying DRN^{DA} neurons and data from both mouse lines were pooled. Recordings of DRN^{DA} neurons revealed distinctive electrophysiological properties such as a slowly ramping membrane potential during constant current injections giving rise to delayed spiking and postinhibitory hypoexcitability (**Figure 1E**). Moreover, most DRN^{DA} neurons displayed rebound oscillations and sag currents (**Figure 1E, F**).

When comparing the electrophysiological properties of DRN^{DA} to $DRN^{5\text{-}HT}$ neurons, we observed numerous differences between these two cell types, but here we focus on the five most significant ones. While $DRN^{5\text{-}HT}$ neurons spike with short delays in response to current steps and maintain a relatively constant action potential (AP) amplitude, DRN^{DA} neurons display a longer delay to the first spike and the amplitude of subsequent APs drops (**Figure 1F-I**). Additionally, the APs of

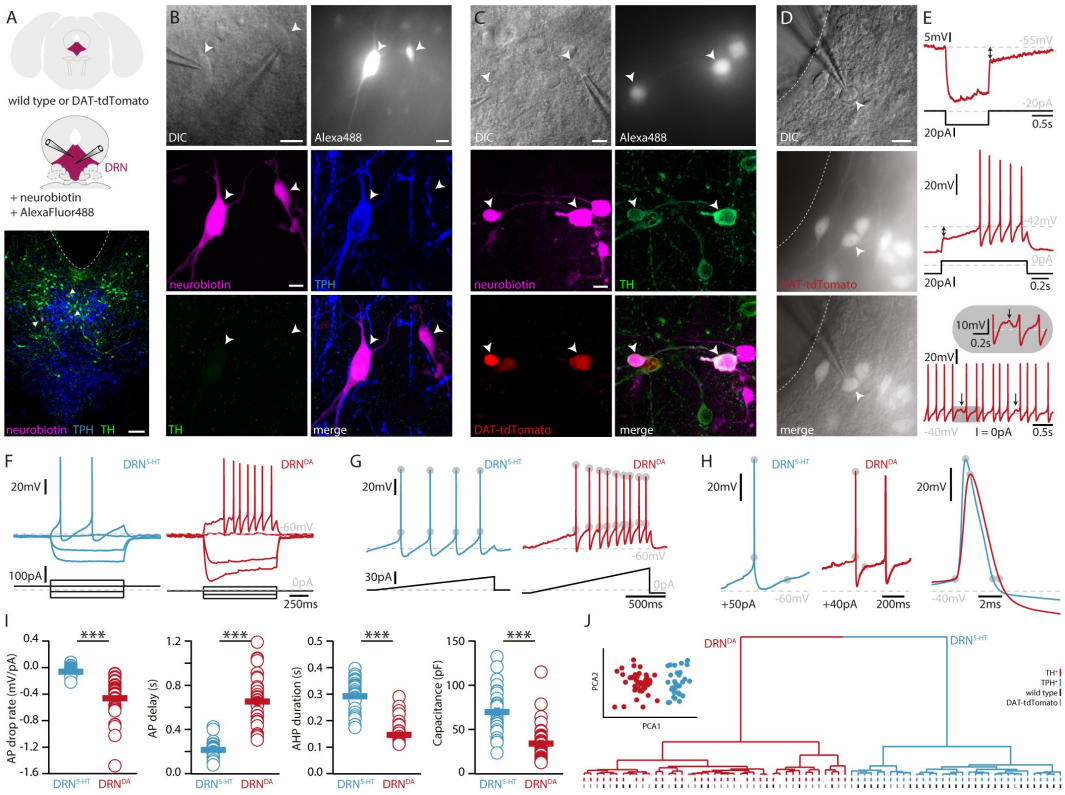

Figure 1.

DRN^{DA} and DRN$^{5\text{-}HT}$ are electrophysiologically distinct cell-types.

(**A**) Scheme of the location of the DRN (pink) in a coronal section (top) and at higher magnification together with two patch pipettes (center). Bottom: a representative slice stained post recording for TPH, TH and neurobiotin revealing serotonergic neurons (arrows). The ventricle is indicated with a dashed line. (**B**) Top: differential interference contrast (DIC) microscopy image (left) of neurons that were filled with Alexa488 (right) and neurobiotin. Center, bottom: staining of the same neurons revealing a TPH+ (DRN$^{5\text{-}HT}$) neuron and a TPH- and TH- cell. (**C**) Top: DIC image of recorded neurons that were filled with Alexa488 and neurobiotin. Center, bottom: staining of the same neurons revealing tdTomato- and TH+ (DRN^{DA}) neurons. (**D**) Representative fluorescent (top), DIC (center) image and overlay (bottom) of a tdTomato+ neuron in a DAT-tdTomato mouse. (**E**) Representative recordings depicting postinhibitory hypoexcitability, slowly ramping currents and rebound oscillations in DRN^{DA} neurons. (**F**) Representative voltage responses to current injections in a TPH+ (DRN$^{5\text{-}HT}$) and TH+ (DRN^{DA}) neuron. (**G**) Ramping current injections reveal action potential (AP) amplitude accommodation. Gray circles indicate the onset and peak of APs. (**H**) Amplitude and duration of the AP and AP afterhyperpolarization (AHP) in a DRN$^{5\text{-}HT}$ and DRN^{DA} neurons. Gray circles indicate onset, peak, and end of the AP and AHP. (**I**) Quantification of electrophysiological properties distinguishing DRN$^{5\text{-}HT}$ from DRN^{DA} neurons (AP drop rate: n = 32 DRN$^{5\text{-}HT}$, n = 43 DRN^{DA}, Capacitance: n = 32 DRN$^{5\text{-}HT}$, n = 43 DRN^{DA}, AP delay: n = 30 DRN$^{5\text{-}HT}$, n = 43 DRN^{DA}, AHP duration: n = 28 DRN$^{5\text{-}HT}$, n = 32 DRN^{DA}, N = 9; Wilcoxon Rank Sum Test). (**J**) Principal component analysis (PCA) of five electrophysiological parameters (insert) and hierarchical cluster analysis based on PCA1 and PCA2 (Ward's method, Euclidean distance). Intrinsic properties were sufficient to separate TPH+ cells (blue dash) from TH+ (red dash) cells. Bottom dashes indicate wild type (black) and DAT-tdTomato (gray) mice. Data are shown as mean ± SEM, ***p < 0.001. Scale bars: A, 100 µm; B-D, 10 µm.

$DRN^{5\text{-}HT}$ neurons rise faster, while their afterhyperpolarization (AHP) is longer compared to DRN^{DA} neurons (**Figure 1H, I**). Lastly, the capacitance of $DRN^{5\text{-}HT}$ neurons is significantly larger than in DRN^{DA} neurons (**Figure 1I**).

Next, we tested if DRN^{DA} neurons can be distinguished from $DRN^{5\text{-}HT}$ neurons based on these five electrophysiological parameters. To this end, we standardized the data and ran a principal component analysis (PCA) including all $DRN^{5\text{-}HT}$ neurons (i. e. all TPH-positive, TPH+), all TH+ neurons recorded in wild-type mice and all tdTomato+ cells recorded in DAT-tdTomato mice (except for one outlier shown in Suppl. Figure 2F, G). Plotting the first two principal components (PC) showed two separate clusters (**Figure 1J**, insert). Unsupervised hierarchical cluster analysis based on PC1 and PC2 revealed the same two major clusters and potential subclusters (**Figure 1J**). Mapping the molecular identity of the cells onto the dendrogram revealed the separation of $DRN^{5\text{-}HT}$ and DRN^{DA} neurons, while there was no branching according to mouse line (wild type vs. DAT-tdTomato), further corroborating the validity of DAT-tdTomato mice as a marker for DRN^{DA} neurons. Overall, these data suggest that electrophysiological parameters themselves are sufficient to distinguish between $DRN^{5\text{-}HT}$ and DRN^{DA} neurons.

In addition to DRN^{DA} and $DRN^{5\text{-}HT}$ the DRN contains an unknown number of cell types and 47 out of 120 recorded neurons were neither TH+, nor TPH+ and did not express tdTomato. To test whether DRN^{DA} can also be distinguished from those populations based on their electrophysiological profile, we ran a PCA on 20 standardized parameters and used the first three PCAs for unsupervised hierarchical clustering (Suppl. Figure 3). Our analysis suggests that there might be four major electrophysiological cell types in the DRN. In contrast to DRN^{DA} and $DRN^{5\text{-}HT}$ neurons, a large proportion of the remaining cells showed rebound spiking and biphasic AHPs, resembling the profiles of local interneurons in other brain areas (Suppl. Figure 3D, E). Interestingly, the clustering also indicated that three TH- and tdTomato-negative (tdTomato-) neurons belonged to the DRN^{DA} neurons and further analysis showed that they were indistinguishable from molecularly identified DRN^{DA} neurons (Suppl. Figure 3C, F). These findings indicate that clustering can be used to identify neurons that otherwise would have been excluded due to a lack of post-hoc staining data or genetic driver lines.

Overall, our data show that DRN^{DA} neurons constitute an electrophysiologically distinct class of neurons in the DRN expressing several hallmark properties, which are sufficient to identify them within the local DRN circuitry.

DRN^{DA} and $DRN^{5\text{-}HT}$ neurons have different morphological properties

Next, we characterized the morphological profile of $DRN^{5\text{-}HT}$ and DRN^{DA} neurons. We focused on the analysis of somatic and dendritic properties since a complete reconstruction of the axonal arborization could not be retrieved from the slices. The analysis of the somatic properties showed that $DRN^{5\text{-}HT}$ neurons had larger cell bodies than DRN^{DA} neurons (**Figure 2A, B**), as measured in their area, perimeter, length, and width (**Figure 2B**). Cell bodies also differed in shape, with DRN^{DA} neurons having more circular somata than $DRN^{5\text{-}HT}$ neurons, as indicated by the circularity index (**Figure 2B**). Analyzing the dendritic properties, we found that $DRN^{5\text{-}HT}$ neurons had four to five primary dendrites, compared to only two to three in DRN^{DA} neurons (**Figure 2A, C**). Moreover, dendrites of DRN^{DA} neurons were frequently bipolar with the main primary dendrites starting from opposite extremes of the soma. Both populations had relatively few bifurcations (**Figure 2C**), but the $DRN^{5\text{-}HT}$ neurons had significantly more terminations (**Figure 2C**). The overall dendritic length did not differ between the $DRN^{5\text{-}HT}$ and DRN^{DA} neurons: both populations had a mix of short and long dendrites (**Figure 2C**). These data suggest that $DRN^{5\text{-}HT}$ neurons have denser dendritic arborization than DRN^{DA} neurons, mostly due to larger numbers of primary dendrites.

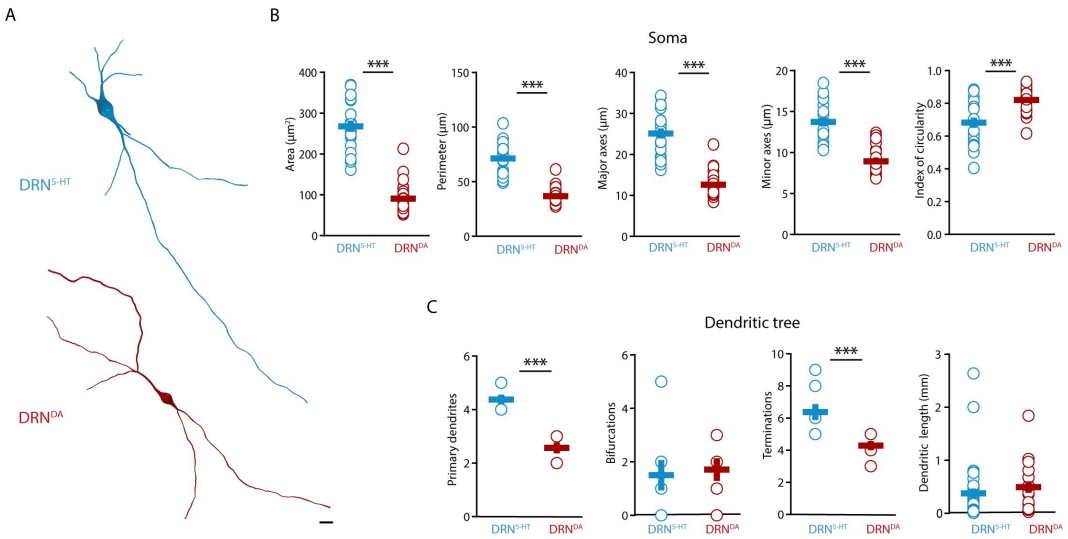

Figure 2.

DRN^{DA} and DRN$^{5\text{-}HT}$ have distinct morphological profiles.

(**A**) Top: representative digital reconstruction of a DRN$^{5\text{-}HT}$. Bottom: representative digital reconstruction of a DRN^{DA}. (**B-F**) Morphological parameters describing the soma size and shape of DRN$^{5\text{-}HT}$ and DRN^{DA} neurons (DRN$^{5\text{-}HT}$: n = 20, N = 3; DRN^{DA}: n = 27, N = 3; Mann-Whitney U test). (**G-J**) Morphological parameters describing the dendritic tree of DRN$^{5\text{-}HT}$ and DRN^{DA} neurons (DRN$^{5\text{-}HT}$: n = 8, N = 3; DRN^{DA}: n = 7, N = 3; Mann-Whitney U test). Data are shown as mean ± SEM, ***p < 0.001. Scale bar: 10 µm.

Altogether, our results show that $DRN^{5\text{-}HT}$ and DRN^{DA} neurons have distinct morphological properties. $DRN^{5\text{-}HT}$ neurons are mostly multipolar neurons, with a big and complex soma and multiple primary dendrites, while DRN^{DA} neurons have smaller and more circular cell bodies with bipolar dendrites.

DA and NA depletion distinctly affect the membrane properties of $DRN^{5\text{-}HT}$ neurons

To elucidate how $DRN^{5\text{-}HT}$ and DRN^{DA} neurons might be affected in PD, we characterized these populations in a mouse model of PD based on bilateral injection of the neurotoxin 6-OHDA in the dorsal striatum. This approach leads to a partial lesion of catecholamine neurons, reproducing an early stage of parkinsonism in which particularly non-motor symptoms such as depression- and anxiety-like behavior are manifested [48, 49]. In line with previous studies, we observed a 60-70% reduction of TH levels in the striatum (Suppl. Figure 4, [50]). Only mice meeting this criterion were included in the study. Measurement performed by ELISA showed that the 6-OHDA injection did not alter the levels of 5-HT in the striatum (Suppl. Figure 4D), and immunostaining showed that the striatal 6-OHDA injection did not cause degeneration of $DRN^{5\text{-}HT}$ or DRN^{DA} neurons (Suppl. Figure 5).

Striatal injection of 6-OHDA has also been found to produce a partial loss of NA neurons in the LC [50] and ELISA analysis showed that this approach induces approximately 60% loss of NA in the striatum (Suppl. Figure 4E). In the present study, we determined the specific impact of NA dysfunction on the physiology of $DRN^{5\text{-}HT}$ and DRN^{DA} neurons by pre-treating a group of mice with desipramine (DMI), a selective inhibitor of NA reuptake, before injecting 6-OHDA (DMI+6-OHDA mice), which partially prevents striatal NA loss (Suppl. Figure 4E). We then assessed the intrinsic properties of $DRN^{5\text{-}HT}$ and DRN^{DA} neurons in Sham-lesion (Sham), 6-OHDA- and DMI+6-OHDA-treated mice. Whole-cell recordings obtained from $DRN^{5\text{-}HT}$ neurons in control mice revealed that 36% of $DRN^{5\text{-}HT}$ neurons were spontaneously active in slices and the proportion of intrinsically active neurons was similar in mice injected with 6-OHDA (Sham: n = 12/33 $DRN^{5\text{-}HT}$ neurons, 6-OHDA: n = 7/18 $DRN^{5\text{-}HT}$ neurons, **Figure 3A**). However, $DRN^{5\text{-}HT}$ neurons recorded in DMI+6-OHDA mice showed an increased excitability: in this condition, 73% of $DRN^{5\text{-}HT}$ neurons were spontaneously active and $DRN^{5\text{-}HT}$ neurons displayed lower rheobase currents than in control and 6-OHDA mice (**Figure 3A, B**). Since the noradrenergic system is protected by DMI in these mice, these findings suggest that the 6-OHDA induced lesion of midbrain dopaminergic neurons evoked the increased firing of $DRN^{5\text{-}HT}$ neurons.

While the excitability of $DRN^{5\text{-}HT}$ neurons was not affected in 6-OHDA mice, we observed that their firing properties were profoundly altered: $DRN^{5\text{-}HT}$ neurons recorded in 6-OHDA mice displayed significantly smaller and shorter APs and AHPs compared to Sham mice (**Figure 3C-E**). Moreover, $DRN^{5\text{-}HT}$ neurons fired at higher frequencies and with shorter delays in response to current injections (**Figure 3F-H**). Finally, the membrane time constant of $DRN^{5\text{-}HT}$ neurons was shorter in 6-OHDA injected mice than in Sham mice (**Figure 3I**). Interestingly, these changes were not observed in 6-OHDA injected mice pre-treated with DMI, suggesting that the noradrenergic lesion critically contributes to the changes in the firing properties of $DRN^{5\text{-}HT}$ neurons in 6-OHDA mice. Taken together, these results indicate that $DRN^{5\text{-}HT}$ neurons are affected in the 6-OHDA mouse model of PD. Specifically, lesions of the dopaminergic system increase the excitability of $DRN^{5\text{-}HT}$ neurons whereas the combined lesion of the noradrenergic and dopaminergic systems changes the firing properties of $DRN^{5\text{-}HT}$ neurons.

Striatal DA depletion induces hypotrophy of $DRN^{5\text{-}HT}$ neurons

Morphological analysis revealed a reduced soma size of the $DRN^{5\text{-}HT}$ neurons in 6-OHDA mice, which was manifested as decreased area, perimeter, and major axes in comparison to control mice (**Figure 4A-C**). Moreover, the increase in the circularity of the 6-OHDA group indicated that

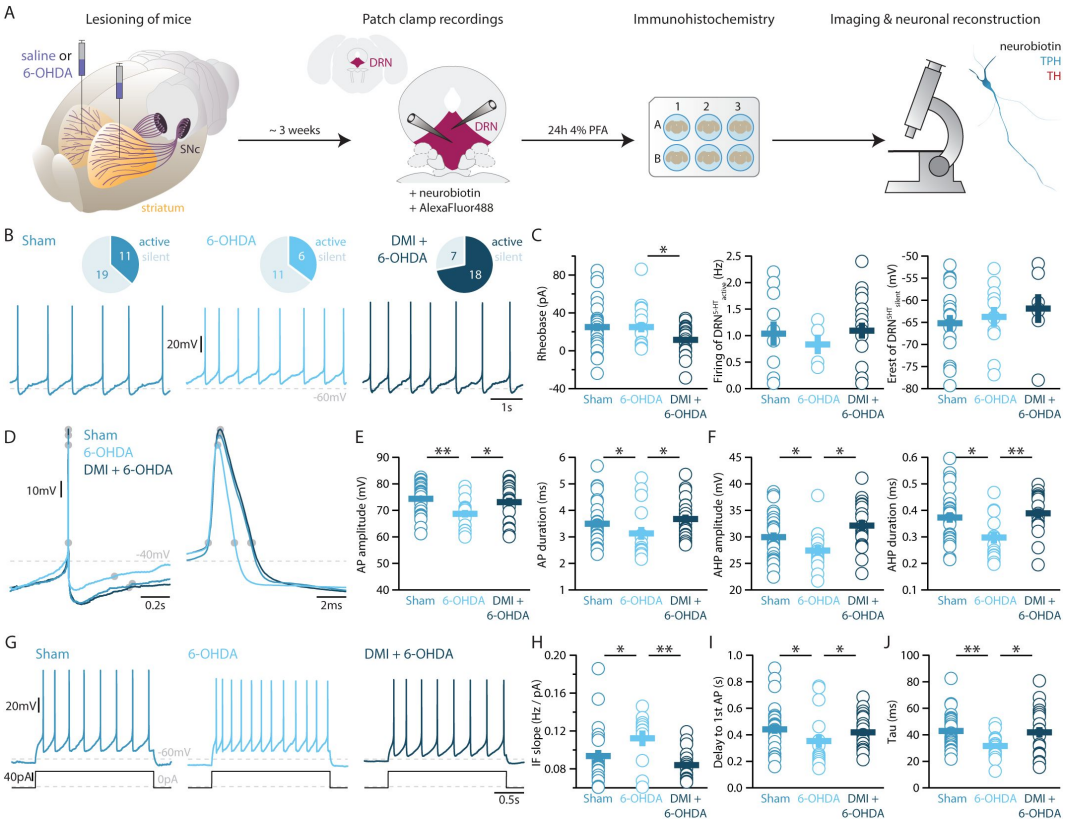

Figure 3.

Lesions targeting primarily nigrostriatal dopamine increase the excitability of DRN$^{5\text{-HT}}$ neurons whereas loss of NA affects their action potentials.

(**A**) Overview of workflow for analyzing the electrophysiological and morphological properties of DRN neurons in Sham and 6-OHDA lesioned mice. (**B**) Top: pie charts showing the number of spontaneously active (dark) and silent (pale) DRN$^{5\text{-HT}}$ neurons in three conditions: Sham (left), 6-OHDA-injected mice (center) and 6-OHDA-injected mice pre-treated with desipramine (DMI + 6-OHDA, right). Bottom: representative recordings of spontaneously active DRN$^{5\text{-HT}}$ neurons (I = 0 pA). (**C**) Quantification of the rheobase (left, Sham: n = 32, 6-OHDA: n = 17, DMI + 6-OHDA: n = 25), the firing frequency of spontaneously active cells (center, Sham: n = 11, 6-OHDA: n = 6, DMI + 6-OHDA: n = 18), and the resting membrane potential of silent DRN$^{5\text{-HT}}$ neurons (right, Sham: n = 19, 6-OHDA: n = 11, DMI + 6-OHDA: n = 7). (**D**) Representative action potentials of DRN$^{5\text{-HT}}$ at low (left) and high (right) temporal resolution. Gray circles indicate onset, offset, and peak of the APs as well as the end of the afterhyperpolarization (AHP). (**E**) Quantification of the amplitude (left) and duration (right) of the APs of DRN$^{5\text{-HT}}$ neurons (Sham: n = 29, 6-OHDA: n = 16, DMI + 6-OHDA: n = 21). (**F**) Same as in (**D**) for the AHP. (**G**) Representative responses of DRN$^{5\text{-HT}}$ neurons to current steps (I = +75 pA). (**H**) Quantification of firing frequency / injected current. (**I**) Quantification of the delay to the first AP when injected with current eliciting 1Hz firing (Sham: n = 29, 6-OHDA: n = 16, DMI + 6-OHDA: n = 21). (**J**) Quantification of the membrane time constant (tau) of DRN$^{5\text{-HT}}$ neurons (Sham: n = 32, 6-OHDA: n = 16, DMI + 6-OHDA: n = 21). Sham: N = 6 - 7; 6-OHDA: N = 7; DMI + 6-OHDA: N = 4; unpaired t-test or Mann-Whitney U test. Data are shown as mean ± SEM, * $p < 0.05$, ** $p < 0.01$.

the shape of the soma of $DRN^{5\text{-}HT}$ neurons was also altered by the lesion (**Figure 4C**). These modifications were not observed in DMI + 6-OHDA mice, suggesting that preserving the NA system protected the $DRN^{5\text{-}HT}$ neurons (Figure4A-C). Finally, the injection of 6-OHDA also caused a significant reduction in the number of primary dendrites of $DRN^{5\text{-}HT}$ neurons in the 6-OHDA group and a tendency to fewer termination points (**Figure 4D**). The number of bifurcations and the dendritic length were not affected by the lesion (**Figure 4D**). Globally, these results suggest that the lesion produced by 6-OHDA induces a hypotrophic phenotype in $DRN^{5\text{-}HT}$ neurons characterized by a shrinkage of the soma and a decrease in dendritic branching and that these alterations are partly NA-dependent.

Striatal DA depletion affects the firing of DRN^{DA} neurons independent of NA loss

Finally, we assessed whether the striatal 6-OHDA lesion affects the physiology of DRN^{DA} neurons. Whole-cell patch-clamp recordings revealed that 58% of DRN^{DA} neurons are spontaneously active in slices of Sham-lesion mice (**Figure 5A**). In contrast, the proportion of intrinsically active neurons increased to 77% and 78% of DRN^{DA} neurons in 6-OHDA injected mice with and without pre-treatment with DMI, respectively. In line with this, silent DRN^{DA} neurons recorded in DMI + 6-OHDA mice were also found to have more depolarized resting membrane potentials and hence to be closer to AP threshold (**Figure 5B**). Yet, active DRN^{DA} neurons tended to fire at lower frequencies in all 6-OHDA mice compared to control mice.

In stark contrast to $DRN^{5\text{-}HT}$ neurons, the APs and AHPs of DRN^{DA} neurons were not affected in any 6-OHDA mice (**Figure 5C-E**). In fact, we did not observe any change in the firing properties of DRN^{DA} neurons that were dependent on the protection of the NA system with DMI (**Figure 5**). Like $DRN^{5\text{-}HT}$ neurons, DRN^{DA} neurons displayed a reduction in spike latency in 6-OHDA mice, but the shortening of the delay was also present in DMI+6-OHDA mice. Together, these results suggest that the electrophysiological properties of DRN^{DA} neurons are affected in the 6-OHDA mouse model of PD and that these changes are primarily due to the lesion of the nigrostriatal dopaminergic pathway.

Striatal DA depletion increases soma complexity and dendritic branching in DRN^{DA} neurons

The morphological analysis of DRN^{DA} neurons revealed that the striatal 6-OHDA injection caused a significant reduction of the circularity from 0.82 (Sham) to 0.77 (6-OHDA) (**Figure 6A-C**), indicating increased complexity of the DRN^{DA} soma. We also observed that this effect was not present in the mice pre-treated with DMI (**Figure 6C**). The soma size was not affected by the lesion and no changes in the area, perimeter, length, and width were found (**Figure 6C**). However, dendritic branching, as shown by the increase in termination points and bifurcations in DRN^{DA} neurons was increased in 6-OHDA-injected mice, but not in mice treated with a combination of DMI and 6-OHDA (**Figure 6D**). The number of primary dendrites and the overall dendritic length were not affected by the 6-OHDA lesion (**Figure 6D**). Overall, these data suggest that impairment of noradrenergic function caused by the striatal 6-OHDA injection altered the soma shape and dendritic branching of DRN^{DA} neurons.

Unilateral lesion of LC NA cells induces minor changes in DRN subpopulations

Our results so far suggest that concomitant lesioning of the DA and NA system (6-OHDA model) has a severe impact on $DRN^{5\text{-}HT}$ neurons which cannot be evoked when the NA system is partially protected (DMI + 6-OHDA model). Therefore, we next assessed if selective lesioning of the NA

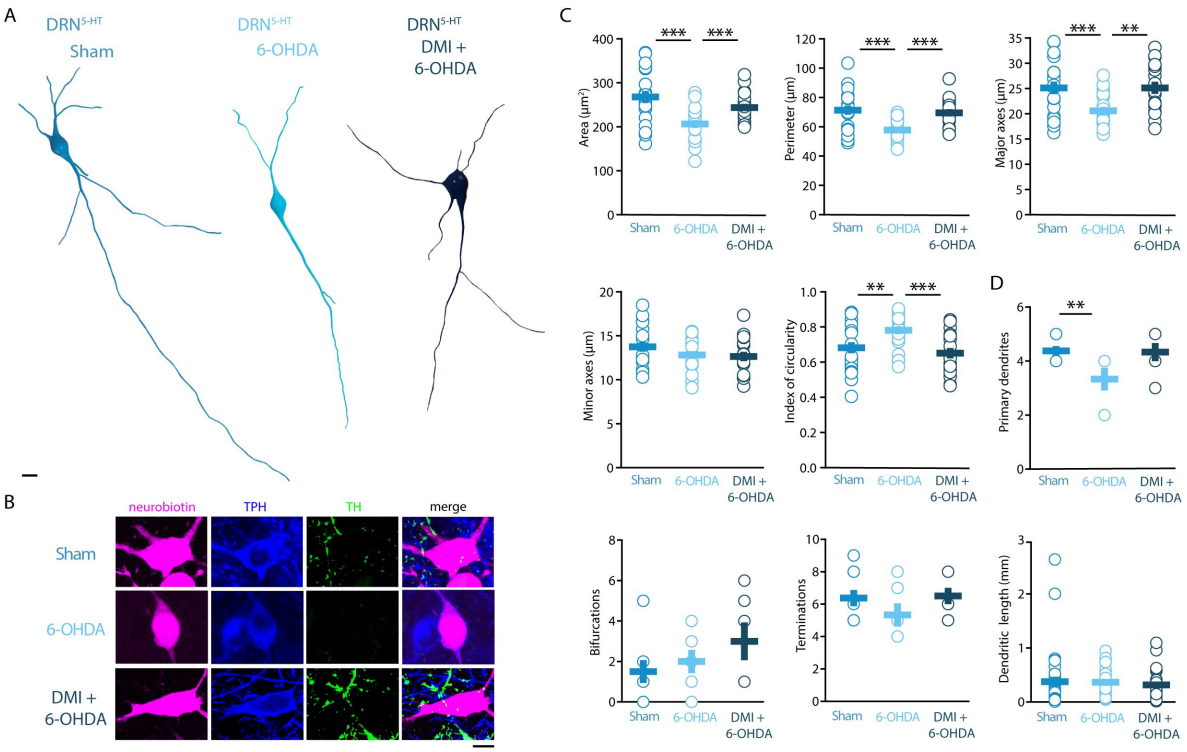

Figure 4.

Striatal injection of 6-OHDA induced a hypotrophic phenotype in the DRN$^{5\text{-HT}}$, which is prevented by pre-treatment with DMI.

(**A**) Representative digital reconstructions of a DRN$^{5\text{-HT}}$ neuron in three different conditions: Sham (left), 6-OHDA-injected mice (center) and 6-OHDA-injected mice pre-treated with desipramine (right). (**B**) Representative confocal pictures of soma from DRN$^{5\text{-HT}}$ neurons in Sham (top), 6-OHDA-injected mice (center), and 6-OHDA-injected mice pre-treated with desipramine (bottom). (**C-G**) Morphological descriptors of the soma size and shape in DRN$^{5\text{-HT}}$ neurons (Sham: n = 20, N = 4; 6-OHDA: n = 19, N = 4; DMI + 6-OHDA: n = 17, N = 3; Mann-Whitney U test). (**H-K**) Morphological descriptors of the dendritic tree in DRN$^{5\text{-HT}}$ neurons (Sham: n = 8, N = 3, 6-OHDA: n = 6, N = 3: DMI + 6-OHDA: n = 6, N = 2; Mann-Whitney U test). Data are shown as mean ± SEM, ***p<0.001, **p<0.01. Scale bar: 10 µm.

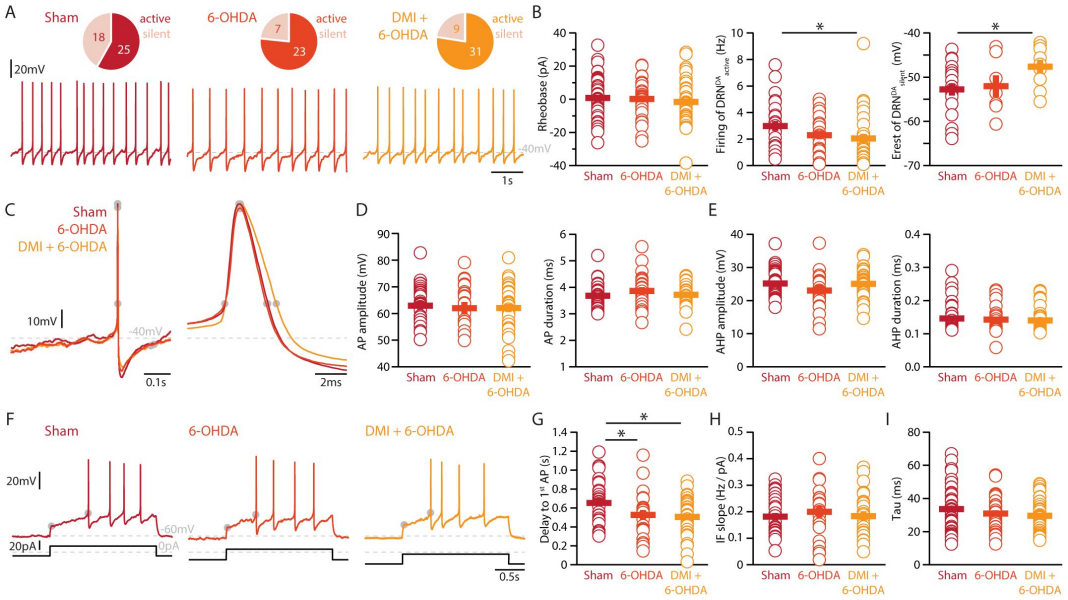

Figure 5.

Lesions targeting primarily SN dopamine depolarize DRN^{DA} neurons whereas concomitant loss of NA does not affect their action potentials.

(**A**) Top: Pie charts showing the proportion of spontaneously active (dark) and silent (pale) DRN^{DA} neurons in three conditions: Sham (left), 6OHDA-injected mice (center) and 6-OHDA-injected mice pre-treated desipramine (DMI, right). Bottom: Representative recordings of spontaneously active DRN^{DA} (I = 0pA). (**B**) Quantification of the rheobase (left, Sham: n = 43, 6-OHDA: n = 31, DMI + 6-OHDA: n = 40), the firing frequency of spontaneously active (center, Sham: n = 25, 6-OHDA: n = 23, DMI + 6-OHDA: n = 31), and the resting membrane potential of silent DRN^{DA} neurons (right, Sham: n = 18, 6-OHDA: n = 7, DMI + 6-OHDA: n = 9). (**C**) Representative action potentials of DRN^{DA} at low (left) and high (right) temporal resolution. Gray circles indicate onset, offset, and peak of APs and the end of the afterhyperpolarization (AHP). (**D**) Quantification of the amplitude (left) and duration (right) of the APs of DRN^{DA} neurons (Sham: n = 34, 6-OHDA: n = 23, DMI + 6-OHDA: n = 35). (**E**) Same as in (D) for the AHP. (**F**) Representative responses of DRN^{DA} neurons to current steps (I = 75pA). Gray circles indicate the delay to the first AP. (**G-I**) Quantification of firing frequency / injected current (G, Sham: n = 31, 6-OHDA: n = 23, DMI + 6-OHDA: n = 27), the delay to the first AP when injected with current eliciting 2 Hz firing (H, Sham: n = 34, 6-OHDA: n = 23, DMI + 6-OHDA: n = 35), and the membrane time constant (I, Sham: n = 43, 6-OHDA: n = 29, DMI + 6-OHDA: n = 40) of DRN^{DA} neurons recorded (Sham: N = 8; 6-OHDA: N = 6; DMI + 6-OHDA: N = 6; unpaired t-test or Mann-Whitney U test). Data are shown as mean ± SEM, * $p < 0.05$.

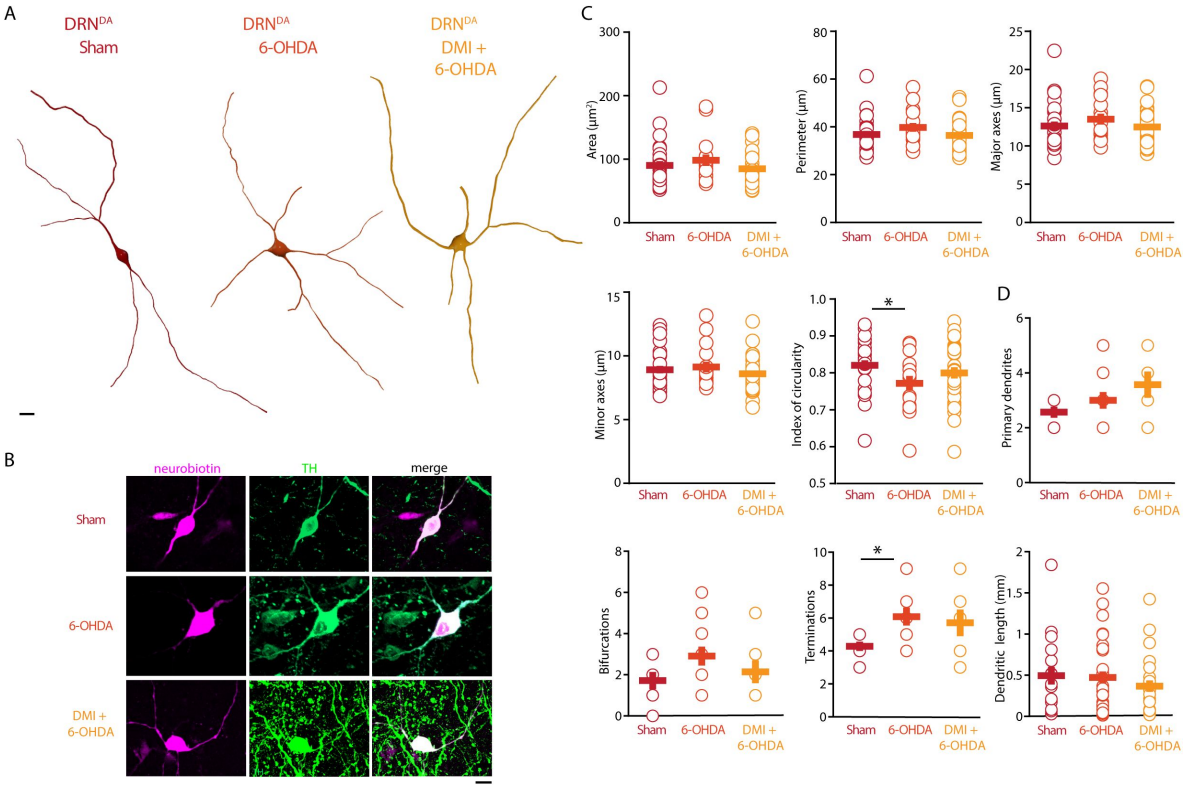

Figure 6.

Striatal injection of 6-OHDA increased soma complexity and branching in DRN^{DA}.

(**A**) Representative digital reconstructions of a DRN^{DA} neuron in three different conditions: Sham (left), 6-OHDA-injected mice (center) and 6-OHDA-injected mice pre-treated with desipramine (right). (**B**) Representative confocal pictures of soma from DRN^{DA} neurons in Sham (top), 6-OHDA-injected mice (center), and 6-OHDA-injected mice pre-treated with DMI (bottom). (**C-G**) Morphological descriptors of the soma size and shape in DRN^{DA} neurons (Sham: n = 27, N = 7, 6-OHDA: n = 16, N = 4; DMI + 6-OHDA: n = 31, N = 5; Mann-Whitney U test). (**H-K**) Morphological descriptors of the dendritic tree in DRN^{DA} neurons. (Sham: n = 7, N = 3; 6-OHDA: n = 11, N = 4; DMI + 6-OHDA: n = 7, N = 3; Mann-Whitney U test). Data are shown as mean ± SEM, *p<0.05. Scale bar: 10 µm.

system itself is sufficient to evoke changes in electrical and morphological properties observed in $DRN^{5\text{-}HT}$ neurons recorded in 6-OHDA. To that end we performed unilateral injections of 6-OHDA/saline in the LC (Suppl. Figure 6A), which lead to approximately 50% loss of TH+ neurons in the LC (Suppl. Figure 6B, C). We chose to restrict the injection of 6-OHDA to one hemisphere because little is known about this type of lesion while the fundamental role of the NA system in various neural processes is well established [51, 52]. We found that selective lesioning of the LC ('6-OHDA-LC') did not alter the baseline activity levels, firing frequencies and resting membrane potentials of $DRN^{5\text{-}HT}$ and DRN^{DA} neurons (Suppl. Fig. 6D, E, K, L). However, $DRN^{5\text{-}HT}$ neurons recorded in 6-OHDA-LC had a lower input resistance at hyperpolarized membrane potentials, a shorter afterhyperpolarization and a larger capacitance than $DRN^{5\text{-}HT}$ neurons recorded in control mice (Sham-LC, Suppl. Fig. 6E-G). Moreover, DRN^{DA} neurons recorded in 6-OHDA-LC showed a reduction in their sag amplitudes (Suppl. Fig 6M, N). The other electrophysiological parameters were not significantly affected. Morphological analysis revealed that the selective lesion of the noradrenergic system did not alter the size and shape of cell bodies in either DRN subpopulation (Suppl. Figure 6H,I, O,P), however, the dendritic branching of both subpopulations was altered, as shown by the increased length of primary dendrites in $DRN^{5\text{-}HT}$neurons (Suppl. Figure 6J) and the increased number of primary dendrites in DRN^{DA} neurons (Suppl. Figure 6Q).

Discussion

In the present study we combine *ex vivo* whole-cell patch clamp recordings with morphological reconstructions and immunohistochemistry, to show that DRN^{DA} neurons have a distinct electrophysiological profile, which is sufficient to distinguish them from $DRN^{5\text{-}HT}$ neurons as well as other neuron classes in the DRN. Utilizing this approach, we also reveal that, in a 6-OHDA mouse model of PD, $DRN^{5\text{-}HT}$ neurons display distinct pathophysiological changes depending on the loss of DA and NA. Notably, degeneration of noradrenergic neurons affects not only the electrical properties of $DRN^{5\text{-}HT}$ neurons but also evokes hypotrophy of their cell bodies. In contrast, the loss of nigrostriatal DA mainly affects the electrophysiological properties of DRN^{DA} neurons while concomitant loss of NA alters their morphology.

We used an extensive electrophysiological characterization protocol to quantify the differences between the DRN^{DA} and $DRN^{5\text{-}HT}$ populations. The electrophysiological properties agree with previous studies, such as the spontaneous firing pattern seen in DRN^{DA} neurons [37], and the slow AHP of $DRN^{5\text{-}HT}$ neurons [23]. Standard electrophysiological parameters were used to create a classification tool, which efficiently identifies $DRN^{5\text{-}HT}$ and DRN^{DA} cells, including DA neurons confirmed by TH staining and / or by fluorescent expression in DAT-tomato mice (**Figure 1**). Importantly, the DRN^{DA} neurons recorded from wild-type and DAT-tdTomato mice did not differ in their electrical properties, indicating that the transgene does not interfere with the membrane properties of this population.

We showed that DRN^{DA} neurons share electrophysiological properties with other dopaminergic populations in the midbrain such as postinhibitory hypoexcitability, rebound oscillations, a slowly ramping membrane potential and sag currents [37, 53, 54], yet their electrophysiological profile is distinct from $DRN^{5\text{-}HT}$ neurons as well as other neuronal populations in the DRN. Most of the parameters extracted in our characterization rely on intracellular recordings of the membrane potential. However, some properties such as spontaneous firing and AP kinetics could be useful for *in vivo* characterization, even in extracellular recordings [55–57]. In addition to the $DRN^{5\text{-}HT}$ and DRN^{DA} neuronal populations, a large fraction of neurons displayed electrophysiological properties that were distinct from these two groups (Suppl. Figure 3), suggesting that there are other neuronal subtypes in the DRN network, such as previously reported GABAergic, glutamatergic, and peptidergic neurons [9, 10, 58–62].

In line with previous studies, the majority of DRN$^{5\text{-HT}}$ neurons were large multipolar or fusiform neurons with four to five primary dendrites, very distinct from the DRN^{DA} neurons [63–65]. Very little is known about the morphology of the DRN^{DA} neurons, but previous studies identified small ovoid cells in the DRN which are likely to correspond to the DRN^{DA} cells [37, 66]. Out of 25 reconstructed DRN$^{5\text{-HT}}$ neurons, only one displayed dendritic spines. Previous studies in rats described the presence of dendritic spines in most DRN$^{5\text{- HT}}$ neurons [67]. However, the study was performed in thicker slices and the dendritic spines were scarce in the primary and secondary dendrites, while they became dense in the distal dendrites, thus it is possible that in our study those dendrites were not present [67].

In the present study we assessed the impact on DRN cells of a striatal bilateral 6-OHDA lesion performed with or without DMI pre-treatment, which has been shown to protect the NA neurons in the LC from the 6-OHDA-induced degeneration [50, 68, 69]. We found that both DRN$^{5\text{-HT}}$ and DRN^{DA} populations were affected in a cell-type specific manner by the combined action of 6-OHDA on DA and NA, with DRN$^{5\text{-HT}}$ neurons being particularly sensitive to changes in the noradrenergic system. Loss of SNc dopaminergic neurons alone (6-OHDA + DMI) – which are known to target DRN$^{5\text{-HT}}$ and DRN^{DA} neurons directly – increased the excitability and spontaneous activity in DRN$^{5\text{-HT}}$ neurons [10]. This is in line with previous *ex vivo* and *in vivo* studies showing that the DRN$^{5\text{-HT}}$ neurons display increased firing rates in rodents pre-treated with DMI and injected with 6-OHDA [23, 70] As hypothesized by Prinz et al. [23], the selective loss of midbrain DA may induce a homeostatic increase in the excitability of DRN$^{5\text{-HT}}$ neurons. Our data contrast with a previous *in vivo* study showing decreased firing activity in DRN$^{5\text{-HT}}$ neurons where injection of 6-OHDA was preceded by treatment with DMI and fluoxetine [24]. This dissimilarity may be related to species-specific (rat vs mouse) and technical (intracerebroventricular vs striatal injections, recordings performed at 10 days vs three weeks after the 6-OHDA injection). Importantly, in the same study identification of DRN$^{5\text{-HT}}$ neurons was not molecularly confirmed and the data may include other spontaneously active DRN neurons. In fact, our recordings show that there are non-serotonergic neurons in the DRN, which are spontaneously active and display a regular, slow firing frequency similar to DRN$^{5\text{-HT}}$ neurons, highlighting the importance of unequivocal identification of DRN cell types.

The present study shows that combined DA and NA lesioning affects DRN$^{5\text{-HT}}$ neurons more profoundly than selective loss of DA (**Figure 3**, **4**). In mice treated with 6-OHDA only, several electrophysiological and morphological properties were altered (**Figure 3**, **4**). The time constant and AHP of DRN$^{5\text{-HT}}$ neurons were shorter and the neurons responded with higher firing frequencies to current injections than in Sham. This finding suggests that the pronounced AHP and long tau of these neurons may act as a “brake” limiting their maximum firing frequency in control conditions and that this brake is reduced when the NA system is lesioned. Future studies are needed to assess if DRN$^{5\text{-HT}}$ neurons in fact fire at higher rates in vivo in mice treated with 6-OHDA. In contrast, such changes in DRN$^{5\text{-HT}}$ neurons were prevented when the NA system was protected by pre-treatment with DMI. These findings indicate an important role for NA as mediator of changes in the activity and properties of DRN$^{5\text{-HT}}$ neurons. The changes produced by the 6-OHDA lesion on the DRN^{DA} population were less pronounced than and different from those in DRN$^{5\text{-HT}}$ neurons. In terms of electrophysiological properties, the observed changes were primarily in the DA only lesion (6-OHDA + DMI), suggesting that unlike DRN$^{5\text{-HT}}$, DRN^{DA} neurons are affected by the loss of midbrain DA rather than the accompanying changes in NA (**Figure 5**). Conversely, the morphological changes produced by 6-OHDA in DRN^{DA} neurons appeared to require a concomitant DA and NA lesion, suggesting a stronger impact of the NA modulation (**Figure 6**). Interestingly, unilateral lesions in the LC did not result in significant alterations in DRN neurons to the extent of the larger striatal lesions (Suppl. Figure 6). Although the trends of some of the electrophysiological parameters, such as the amplitude and duration of the AP and the AHP observed in DRN$^{5\text{-HT}}$ neurons, were similar to those induced by the 6-OHDA only lesion shown in **Figure 3**, the effects were smaller. This could be due to the more limited extent of the

LC injections compared to the striatal ones as well as the unilateral LC vs. bilateral striatal lesioning. These two factors may have reduced the impact of NA depletion and should be further investigated in future studies.

Our results show that DRN neurons are affected by depletion of both DA and NA, thus raising the possibility that non-motor symptoms in PD are a result of the intricate organization of DA and NA neuromodulation as well as the interactions between the different DRN neuronal populations. Moreover, our results highlight the complex interplay in the DRN between NA, DA, and 5-HT, but the precise pathophysiological processes resulting from loss of NA, and specifically the impact on DRN, are yet to be elucidated.

In conclusion, our study provides a quantitative description and classification scheme for two major neuronal populations in the DRN, $DRN^{5\text{-}HT}$ and DRN^{DA} neurons. We identified novel electrophysiological and morphological changes in these populations in response to DA and NA depletion in the basal ganglia. Considering the involvement of DRN and LC in the development of non-motor comorbidities, this study provides useful insights to understand better how these areas are affected in the parkinsonian condition. Moreover, our data pave the way for future experiments to characterize these subpopulations in terms of receptor expression and synaptic connectivity to shed light on their functional roles particularly with regard to the wide variety of non-motor symptoms observed in PD.

Methods

Experimental model details

All animal procedures were performed in accordance with the national guidelines and approved by the local ethics committee of Stockholm, Stockholms Norra djurförsöksetiska nämnd, under ethical permits to G. F. (N12148/17, 14673-22) and G. S. (N2020/2022). All mice (N=43) were group-housed under a 12 hr light / dark schedule and given ad libitum access to food and water. Wild-type mice ('C57BL/6J', #000664, the Jackson laboratory) and DAT-cre (Stock #006660 the Jackson laboratory) mice crossed with homozygous tdTomato reporter mice ('Ai9', stock #007909, the Jackson laboratory) were used.

6-OHDA model

Three-months old, male and female C57BL/6J or DAT-tdTomato were deeply anesthetized with Isoflurane and mounted on a stereotaxic frame (Stoelting Europe, Dublin, Ireland). To achieve a partial striatal lesion, each mouse received a bilateral injection of 1.25 µl of 6-hydroxydopamine hydrochloride (6-OHDA, Sigma-Aldrich, 4µg/µl) or vehicle (0.9 % NaCl + Ascorbic Acid 0.02%) in the dorsolateral striatum, according to the following coordinates: anteroposterior +0.6 mm, mediolateral ± 2.2, dorsoventral −3.2 from Bregma, as previously described [48, 71]. One group of mice (referred to as DMI + 6-OHDA) was pre-treated with one injection of desipramine hydrochloride (DMI, Sigma-Aldrich, 25mg/kg i.p.) 30 minutes before the 6-OHDA infusion in order to protect the noradrenergic system [50].

For the LC lesion, mice received a unilateral injection of 1 µl of 6-OHDA (Sigma-Aldrich, 4µg/µl) or vehicle (0.9 % NaCl + Ascorbic Acid 0.02%) according to the following coordinates: anteroposterior –5.4 mm, mediolateral –0.9, dorsoventral −3.8 from Bregma.

Slice preparation and electrophysiology

Three weeks after the 6-OHDA/vehicle injection, mice were deeply anaesthetized with isoflurane and decapitated. The brain was quickly removed and immersed in ice-cold cutting solution containing 205 mM sucrose, 10 mM glucose, 25 mM NaHCO3, 2.5 mM KCl, 1.25 mM NaH2PO4, 0.5

mM CaCl2 and 7.5 mM MgCl2. In all experiments, the brain was divided into two parts: the striatum was dissected from the anterior section for Western Blot and the posterior part was used to prepare coronal brain slices (250 µm) with a Leica VT 1000S vibratome. Slices were incubated for 30-60 min at 34°C in a submerged chamber filled with artificial cerebrospinal fluid (ACSF) saturated with 95% oxygen and 5% carbon dioxide. ACSF was composed of 125 mM NaCl, 25 mM glucose, 25 mM NaHCO3, 2.5 mM KCl, 2 mM CaCl2, 1.25 mM NaH2PO4, and 1 mM MgCl2. Subsequently, slices were kept for at least 60 min at room temperature before recording. Whole-cell patch clamp recordings were obtained in oxygenated ACSF at 35°C. Neurons were visualized using infrared differential interference contrast (IR-DIC) microscopy (Zeiss FS Axioskop, Oberkochen, Germany). DAT-tdTomato positive cells were identified by switching to epifluorescence using a mercury lamp (X-cite, 120Q, Lumen Dynamics). Up to three cells were patched simultaneously. Borosilicate glass pipettes (Hilgenberg) of 6 - 8 MOhm resistance were pulled with a Flaming / Brown micropipette puller P-1000 (Sutter Instruments). The intracellular solution contained 130 mM K-gluconate, 5 mM KCl, 10 mM HEPES, 4 mM Mg-ATP, 0.3 mM GTP, 10 mM Na2-phosphocreatine (pH 7.25, osmolarity 285 mOsm), 0.2% neurobiotin (Vector laboratories, CA) and Alexa-488 (75 µM) was added to the intracellular solution (Invitrogen). Recordings were made in current-clamp mode and the intrinsic properties of the neurons were determined by a series of hyperpolarizing and depolarizing current steps and ramps, enabling the extraction of sub- and suprathreshold properties. Recordings were amplified using MultiClamp 700B amplifiers (Molecular Devices, CA, USA), filtered at 2kHz, digitized at 10-20kHz using ITC-18 (HEKA Elektronik, Instrutech, NY, USA), and acquired using custom-made routines running on IgorPro (Wavemetrics, OR, USA). Throughout all recordings pipette capacitance and access resistance were compensated for and data were discarded when access resistance increased beyond 30 MOhm. Liquid junction potential was not corrected for.

Quantification of electrophysiological parameters

Immediately after obtaining a whole-cell patch in DRN neurons, we first obtained a 10s voltage recording of the neural activity without injecting any current. This recording was used to calculate the average resting membrane potential in silent neurons and the firing frequency of spontaneously active neurons. Subsequently, neurons were held at –60mV while an extensive series of de- and hyperpolarizing current steps was applied. The amplitude of all current steps was scaled according to a test pulse that was set to evoke one to two AP. The resulting voltage recordings were used to extract and calculate the following parameters: The rheobase was defined as the minimum current required to evoke AP firing. AP parameters were extracted from recordings where $DRN^{5\text{-}HT}$ neurons fired at 1 ± 0.3 Hz and DRN^{DA} neurons at 2 ± 0.3 Hz (i.e. close to their average spontaneous firing frequency) and values from individual APs were averaged. AP onset was extracted by quantifying where the rising slope of the AP (its first derivative) reached 5V/s and the end of the AP was defined as the time where the AP had repolarized to the same membrane voltage as found at the onset. The AP duration was calculated as the time between the onset and the offset. The amplitude of the AP was defined as the voltage difference between the onset and its peak. The amplitude of the AHP was defined as the voltage difference between the end of the AP and the subsequent local minimum. The end of the AHP was found by using a sliding window of 50ms to assess when the slope of the decaying AHP had first decreased to 0.005V/s or less. The AP drop rate was measured by injecting a current ramp into the neurons that evoked multiple APs. The amplitude of these APs was extracted as described above. The amplitude was plotted versus the injected current and a linear fit was applied whose slope constitutes the AP drop rate. The delay to the first spike constitutes the time between the onset of the current injection and the onset of the first AP in recordings. The input resistance was based on the slope of a linear fit across all current–voltage steps that resulted in a steady state voltage between –90 and –50mV (R = U / I). The steady state voltage was based on the average voltage found during a time window starting 0.5s after the beginning of a 1s long current step and lasting until the end of the current step. The amplitude of sag currents was defined as the average voltage difference between the steady state voltage and the peak voltage evoked by current steps that hyperpolarized the neurons to –90 ± 5mV. The peak voltage constituted the minimum voltage observed during the first

0.5s of the step. The time constant tau was extracted following injection of a 5ms long hyperpolarizing current step. We applied an exponential fit to the resulting voltage recording that started 1ms after the negative voltage peak had been reached and ended when the membrane potential had returned to the average baseline voltage preceding the step. Tau corresponds to K2 given the exponential fit is defined as y = K0 + K1*exp(-K2*x). Based on tau and the steady-state input resistance, we calculated the capacitance C according to C = tau / resistance. The IF slope was extracted from the linear fit applied to a current-frequency plot.

Immunofluorescence

Following the recordings, slices were fixated overnight at 4°C in a 4% paraformaldehyde solution. Slices were then washed with PBS 1X. For the immunofluorescence, slices were treated with PBS 1X + Triton 0.3% and then incubated with a blocking solution of Normal Serum 10% and Bovine Serum Albumin 1% for 1h at room temperature. Afterward, slices were incubated overnight at 4°C with the following primary antibodies: rabbit anti-TH (Millipore, 1:1000), mouse anti-TPH (Sigma Aldrich, 1:600) and Streptavidin (Jackson Immunoresearch, 1:500). The following day, primary antibodies were washed out and slices were incubated with the appropriate fluorochrome-conjugated secondary antibodies.

For the immunostainings in the striatum, SNc, LC and cell counting in DRN, mice were deeply anesthetized and transcardially perfused with PFA 4%. The brains were extracted and post-fixed in PFA 4% for 24 hours. 40 µm coronal slices were prepared with a vibratome (Leica VT1000 S) and processed as described above.

Confocal Microscopy Analysis

The slices were imaged using Confocal (ZEISS LSM 800) at 10X and 40X and z-stacks were retrieved. For cell identification, colocalization between neurobiotin and TH or TPH was evaluated.

Morphological analysis

For morphological analysis of dendrites, the confocal z-stacks were used in a semi-manual reconstruction using neuTube [72] and custom code, as previously described [73]. Soma morphology was analyzed by tracing manually the cell body profile, excluding dendritic trunks, in order to measure area (µm²), perimeter, major and minor axis length (µm) and circularity values. Circularity, calculated as the ratio between the squared perimeter and the area (i.e. perimeter²/4π area), can be a value between 0 and 1 (1 for circular shapes and values < 1 for more complex shapes).

The morphological analysis was performed on the neurobiotin stacks.

Western Blot

The striata were sonicated in 1% sodium dodecyl sulfate and boiled for 10 min. Equal amounts of protein (25 µg) for each sample were loaded onto 10% polyacrylamide gels and separated by electrophoresis and transferred overnight to nitrocellulose membranes (Thermo Fisher, Stockholm, Sweden). The membranes were immunoblotted with primary antibodies against actin (1:30,000, Sigma Aldrich, Stockholm, Sweden) and TH (1:2000, Millipore, Darmstadt, Germany). Detection was based on fluorescent secondary antibody binding (IR Dye 800CW and 680RD, Li-Cor, Lincoln, NE, USA) and quantified using a Li-Cor Odyssey infrared fluorescent detection system (Li-Cor, Lincoln, NE, USA). The TH protein levels were normalized for the corresponding actin detected in the sample and then expressed as a percentage of the control (Sham-lesion).

Enzyme-linked immunosorbent assay

NA and 5-HT levels in the striatum were determined by Enzyme-linked immunosorbent assay (ELISA). Three weeks after the 6-OHDA injection, mice were killed by decapitation and the striatum was dissected out freehand on an ice-cold surface and weighted. The tissue was sonicated in a buffer with HCl 0.01M, EDTA 1mM and sodium metabisulfite 4 mM (25 µl/mg of tissue). The brain homogenates were centrifuged at 4 °C, 13000 rpm for 20 minutes and the supernatants were collected. The samples were assessed in analytic duplicate using Noradrenaline and Serotonin Research ELISA kits (LDN, Germany), according to the manufacturer's instructions. The absorbance at 450 nm was measured using a microplate reader. Tissue concentrations of NA and 5-HT were determined using a standard curve.

Statistical Analysis

Statistical analysis of morphology data was performed using GraphPad Prism 9.2.0 and data were analyzed by the Mann-Whitney U test, while data from WB and ELISA were analyzed by one-way ANOVA. Cell counting data were analyzed by unpaired t-test. Electrophysiological data was first tested for normality (Shapiro-Wilk test) before running an unpaired t-test for normally distributed data and the Mann-Whitney U test for non-normally distributed data in matlab. Data are reported as average ± SEM. N indicates the number of mice, while n indicates the number of cells. Significance was set at $p<0.05$.

Acknowledgements

We thank Elin Dahlberg for technical assistance and Kristoffer Tenebro Berglund for taking care of the mice. We also thank the members of the Silberberg and Fisone labs and the AND-PD consortium members for comments and discussions.

Funding

This work was supported by a Wallenberg Fellowship from the Knut & Alice Wallenberg Foundation (KAW 2017.0273), the Swedish Brain Foundation (Hjärnfonden, FO2021-0333), and the Swedish Medical Research Council (VR-M, 2019-0 1254) to GS, and a Swedish Research Council International Postdoc Grant (2020-06365) to YJ. RT, RA, GF, and GS are supported by an EU grant (H2020 848002 AND-PD).

Author contributions

Conceptualization: LB, YJ, RT, RM, GF, GS.

Investigation: YJ (electrophysiology, clustering analysis), LB (6-OHDA lesions, morphological analysis, cell counting, western blot, ELISA).

Visualization: YJ (electrophysiological and clustering results), LB (6-OHDA model, morphological reconstructions).

Supervision: GS and GF.

Writing—original draft: YJ and LB.

Writing—review & editing: LB, YJ, GF, GS.

Competing Interests

The authors declare that they have no competing interests.

Data availability

All raw data is available upon reasonable request.

References

1. Braak H., et al. (2003) **Staging of brain pathology related to sporadic Parkinson's disease** *Neurobiol Aging* **24**:197–211
2. Jankovic J (2008) **Parkinson's disease: clinical features and diagnosis** *J Neurol Neurosurg Psychiatry* **79**:368–76
3. Swick T.J (2012) **Parkinson's disease and sleep/wake disturbances** *Parkinsons Dis* **2012**
4. Chaudhuri K.R., Schapira A.H. (2009) **Non-motor symptoms of Parkinson's disease: dopaminergic pathophysiology and treatment** *Lancet Neurol* **8**:464–74
5. Halliday G.M., et al. (1990) **Loss of brainstem serotonin- and substance P-containing neurons in Parkinson's disease** *Brain Res* **510**:104–7
6. Halliday G.M., et al. (1990) **Neuropathology of immunohistochemically identified brainstem neurons in Parkinson's disease** *Ann Neurol* **27**:373–85
7. Gesi M., et al. (2000) **The role of the locus coeruleus in the development of Parkinson's disease** *Neurosci Biobehav Rev* **24**:655–68
8. Zarow C., et al. (2003) **Neuronal loss is greater in the locus coeruleus than nucleus basalis and substantia nigra in Alzheimer and Parkinson diseases** *Arch Neurol* **60**:337–41
9. Huang K.W., et al. (2019) **Molecular and anatomical organization of the dorsal raphe nucleus** *Elife* **8**
10. Pollak Dorocic I., et al. (2014) **A whole-brain atlas of inputs to serotonergic neurons of the dorsal and median raphe nuclei** *Neuron* **83**:663–78
11. Soghomonian J.J., Descarries L., Watkins K.C. (1989) **Serotonin innervation in adult rat neostriatum** *II. Ultrastructural features: a radioautographic and immunocytochemical study. Brain Res* **481**:67–86
12. Maillet A., et al. (2021) **Serotonergic and Dopaminergic Lesions Underlying Parkinsonian Neuropsychiatric Signs** *Mov Disord*

13. Jørgensen L.M., et al. (2021) **Parkinson patients have a presynaptic serotonergic deficit: A dynamic deep brain stimulation PET study** *J Cereb Blood Flow Metab* **41**:1954–1963

14. Cheshire P., et al. (2015) **Serotonergic markers in Parkinson's disease and levodopa-induced dyskinesias** *Mov Disord* **30**:796–804

15. Pifl C., Schingnitz G., Hornykiewicz O. (1991) **Effect of 1-methyl-4-phenyl-1,2,3,6-tetrahydropyridine on the regional distribution of brain monoamines in the rhesus monkey** *Neuroscience* **44**:591–605

16. Rylander D., et al. (2010) **Maladaptive plasticity of serotonin axon terminals in levodopa-induced dyskinesia** *Ann Neurol* **68**:619–28

17. Nayyar T., et al. (2009) **Cortical serotonin and norepinephrine denervation in parkinsonism: preferential loss of the beaded serotonin innervation** *Eur J Neurosci* **30**:207–16

18. Taylor T.N., et al. (2009) **Nonmotor symptoms of Parkinson's disease revealed in an animal model with reduced monoamine storage capacity** *J Neurosci* **29**:8103–13

19. Karstaedt P.J., et al. (1994) **Unilateral destruction of dopamine pathways increases ipsilateral striatal serotonin turnover in rats** *Exp Neurol* **126**:25–30

20. Wilson H., et al. (2018) **Serotonergic dysregulation is linked to sleep problems in Parkinson's disease** *Neuroimage Clin* **18**:630–637

21. Politis M., et al. (2010) **Depressive symptoms in PD correlate with higher 5-HTT binding in raphe and limbic structures** *Neurology* **75**:1920–7

22. Kaya A.H., et al. (2008) **Increased electrical and metabolic activity in the dorsal raphe nucleus of Parkinsonian rats** *Brain Res* **1221**:93–7

23. Prinz A., et al. (2013) **Increased excitability in serotonin neurons in the dorsal raphe nucleus in the 6-OHDA mouse model of Parkinson's disease** *Exp Neurol* **248**:236–45

24. Guiard B.P., et al. (2008) **Functional interactions between dopamine, serotonin and norepinephrine neurons: an in-vivo electrophysiological study in rats with monoaminergic lesions** *Int J Neuropsychopharmacol* **11**:625–39

25. Descarries L., et al. (1986) **Dopaminergic projection from nucleus raphe dorsalis to neostriatum in the rat** *J Comp Neurol* **249**:511–20

26. Wenk G.L., et al. (1994) **Behavioral, biochemical, histological, and electrophysiological effects of 192 IgG-saporin injections into the basal forebrain of rats** *J Neurosci* **14**:5986–95

27. Lu J., Jhou T.C., Saper C.B. (2006) **Identification of wake-active dopaminergic neurons in the ventral periaqueductal gray matter** *J Neurosci* **26**:193–202

28. Dzirasa K., et al. (2006) **Dopaminergic control of sleep-wake states** *J Neurosci* **26**:10577–89

29. Cho J.R., et al. (2017) **Dorsal Raphe Dopamine Neurons Modulate Arousal and Promote Wakefulness by Salient Stimuli** *Neuron* **94**:1205–1219

30. Lin R., et al. (2020) **The Raphe Dopamine System Controls the Expression of Incentive Memory** *Neuron* **106**:498–514

31. Matthews G.A., et al. (2016) **Dorsal Raphe Dopamine Neurons Represent the Experience of Social Isolation** *Cell* **164**:617–31

32. Taylor N.E., et al. (2019) **The Role of Glutamatergic and Dopaminergic Neurons in the Periaqueductal Gray/Dorsal Raphe: Separating Analgesia and Anxiety** *eNeuro* **6**

33. Li C., et al. (2016) **Mu Opioid Receptor Modulation of Dopamine Neurons in the Periaqueductal Gray/Dorsal Raphe: A Role in Regulation of Pain** *Neuropsychopharmacology* **41**:2122–32

34. Flores J.A., et al. (2004) **Opiate anti-nociception is attenuated following lesion of large dopamine neurons of the periaqueductal grey: critical role for D1 (not D2) dopamine receptors** *Pain* **110**:205–14

35. Flores J.A., et al. (2006) **Role for dopamine neurons of the rostral linear nucleus and periaqueductal gray in the rewarding and sensitizing properties of heroin** *Neuropsychopharmacology* **31**:1475–88

36. Cardozo Pinto D.F., et al. (2019) **Characterization of transgenic mouse models targeting neuromodulatory systems reveals organizational principles of the dorsal raphe** *Nat Commun* **10**

37. Dougalis A.G., et al. (2012) **Functional properties of dopamine neurons and co-expression of vasoactive intestinal polypeptide in the dorsal raphe nucleus and ventro-lateral periaqueductal grey** *Eur J Neurosci* **36**:3322–3332

38. Fu W., et al. (2010) **Chemical neuroanatomy of the dorsal raphe nucleus and adjacent structures of the mouse brain** *J Comp Neurol* **518**:3464–94

39. Okaty B.W., et al. (2015) **Multi-Scale Molecular Deconstruction of the Serotonin Neuron System** *Neuron* **88**:774–91

40. Lindeberg J., et al. (2004) **Transgenic expression of Cre recombinase from the tyrosine hydroxylase locus** *Genesis* **40**:67–73

41. Lammel S., et al. (2015) **Diversity of transgenic mouse models for selective targeting of midbrain dopamine neurons** *Neuron* **85**:429–38

42. Carter M.E., et al. (2010) **Tuning arousal with optogenetic modulation of locus coeruleus neurons** *Nat Neurosci* **13**:1526–33

43. Pudovkina O.L., Cremers T.I., Westerink B.H. (2003) **Regulation of the release of serotonin in the dorsal raphe nucleus by alpha1 and alpha2 adrenoceptors** *Synapse* **50**:77–82

44. Trulson M.E., Crisp T. (1984) **Role of norepinephrine in regulating the activity of serotonin-containing dorsal raphe neurons** *Life Sci* **35**:511–5

45. Haddjeri N., de Montigny C., Blier P. (1997) **Modulation of the firing activity of noradrenergic neurones in the rat locus coeruleus by the 5-hydroxtryptamine system** *Br J Pharmacol* **120**:865–75

46. Singewald N., et al. (1998) **Influence of excitatory amino acids on basal and sensory stimuli-induced release of 5-HT in the locus coeruleus** *Br J Pharmacol* **123**:746–52

47. Aston-Jones G., et al. (1991) **Serotonin selectively attenuates glutamate-evoked activation of noradrenergic locus coeruleus neurons** *J Neurosci* **11**:760–9

48. Bonito-Oliva A., Masini D., Fisone G. (2014) **A mouse model of non-motor symptoms in Parkinson's disease: focus on pharmacological interventions targeting affective dysfunctions** *Front Behav Neurosci* **8**

49. Ztaou S., et al. (2018) **Striatal cholinergic interneurons regulate cognitive and affective dysfunction in partially dopamine-depleted mice** *Eur J Neurosci* **48**:2988–3004

50. Bonito-Oliva A., et al. (2014) **Cognitive impairment and dentate gyrus synaptic dysfunction in experimental parkinsonism** *Biol Psychiatry* **75**:701–10

51. Poe G.R., et al. (2020) **Locus coeruleus: a new look at the blue spot** *Nat Rev Neurosci* **21**:644–659

52. Szot P., et al. (2012) **Lesioning noradrenergic neurons of the locus coeruleus in C57Bl/6 mice with unilateral 6-hydroxydopamine injection, to assess molecular, electrophysiological and biochemical changes in noradrenergic signaling** *Neuroscience* **216**:143–57

53. Neuhoff H., et al. (2002) **I(h) channels contribute to the different functional properties of identified dopaminergic subpopulations in the midbrain** *J Neurosci* **22**:1290–302

54. Lammel S., et al. (2008) **Unique properties of mesoprefrontal neurons within a dual mesocorticolimbic dopamine system** *Neuron* **57**:760–73

55. Strickland J.A., McDannald M.A. (2022) **Brainstem networks construct threat probability and prediction error from neuronal building blocks** *Nat Commun* **13**

56. Hajós M., et al. (2007) **Neurochemical identification of stereotypic burst-firing neurons in the rat dorsal raphe nucleus using juxtacellular labelling methods** *Eur J Neurosci* **25**:119–26

57. Schweimer J.V., et al. (2011) **Spike-timing relationship of neurochemically-identified dorsal raphe neurons during cortical slow oscillations** *Neuroscience* **196**:115–23

58. Dahlstroem A., Fuxe K. (1964) **EVIDENCE FOR THE EXISTENCE OF MONOAMINE-CONTAINING NEURONS IN THE CENTRAL NERVOUS SYSTEM. I. DEMONSTRATION OF MONOAMINES IN THE CELL BODIES OF BRAIN STEM NEURONS** . *Acta Physiol Scand Suppl* :1–55

59. Weissbourd B., et al. (2014) **Presynaptic partners of dorsal raphe serotonergic and GABAergic neurons** *Neuron* **83**:645–62

60. Gocho Y., et al. (2013) **Electrophysiological and pharmacological properties of GABAergic cells in the dorsal raphe nucleus** *J Physiol Sci* **63**:147–54

61. Xu Z., et al. (2021) **Whole-brain connectivity atlas of glutamatergic and GABAergic neurons in the mouse dorsal and median raphe nuclei** *Elife* **10**

62. Bowker R.M., et al. (1983) **Descending serotonergic, peptidergic and cholinergic pathways from the raphe nuclei: a multiple transmitter complex** *Brain Res* **288**:33–48

63. Rivera H.M., Bethea C.L. (2013) **Ovarian steroids increase PSD-95 expression and dendritic spines in the dorsal raphe of ovariectomized macaques** *Synapse* **67**:897–908

64. Park M.R (1987) **Intracellular horseradish peroxidase labeling of rapidly firing dorsal raphe projection neurons** *Brain Res* **402**:117–30

65. Calizo L.H., et al. (2011) **Raphe serotonin neurons are not homogenous: electrophysiological, morphological and neurochemical evidence** *Neuropharmacology* **61**:524–43

66. Diaz-Cintra S., et al. (1981) **Nucleus raphe dorsalis: a morphometric Golgi study in rats of three age groups** *Brain Res* **207**:1–16

67. Li Y.Q., et al. (2001) **Morphological features and electrophysiological properties of serotonergic and non-serotonergic projection neurons in the dorsal raphe nucleus. An intracellular recording and labeling study in rat brain slices** *Brain Res* **900**:110–8

68. Kamińska K., et al. (2017) **Depressive-like neurochemical and behavioral markers of Parkinson's disease after 6-OHDA administered unilaterally to the rat medial forebrain bundle** *Pharmacol Rep* **69**:985–994

69. Fulceri F., et al. (2006) **Nigrostriatal damage with 6-OHDA: validation of routinely applied procedures** *Ann N Y Acad Sci* **1074**:344–8

70. Wang S., et al. (2009) **Unilateral lesion of the nigrostriatal pathway induces an increase of neuronal firing of the midbrain raphe nuclei 5-HT neurons and a decrease of their response to 5-HT(1A) receptor stimulation in the rat** *Neuroscience* **159**:850–61

71. Masini D., et al. (2021) **A Guide to the Generation of a 6-Hydroxydopamine Mouse Model of Parkinson's Disease for the Study of Non-Motor Symptoms** *Biomedicines* **9**

72. Feng L., Zhao T., Kim J. (2015) **neuTube 1.0: A New Design for Efficient Neuron Reconstruction Software Based on the SWC Format** *eNeuro* **2**

73. Hjorth J.J.J., et al. (2020) **The microcircuits of striatum in silico** *Proc Natl Acad Sci U S A* **117**:9554–9565

Article and author information

Laura Boi
Department of Neuroscience, Karolinska Institutet, Stockholm 17177, Sweden

Yvonne Johansson
Sainsbury Wellcome Centre for Neural Circuits and Behaviour, University College London, London, UK

Raffaella Tonini
Neuromodulation of Cortical and Subcortical Circuits Laboratory, Istituto Italiano di Tecnologia, Genova, Italy

Rosario Moratalla
Cajal Institute, Spanish National Research Council (CSIC), Madrid, Spain, CIBERNED, Instituto de Salud Carlos III, Madrid, Spain

Gilberto Fisone
Department of Neuroscience, Karolinska Institutet, Stockholm 17177, Sweden

Gilad Silberberg
Department of Neuroscience, Karolinska Institutet, Stockholm 17177, Sweden
For correspondence: gilad.silberberg@ki.se
ORCID iD: 0000-0001-9964-505X

Copyright

Editors

Reviewing Editor
Jun Ding
Stanford University, Stanford, United States of America

Senior Editor
John Huguenard
Stanford University School of Medicine, Stanford, United States of America

Reviewer #1 (Public Review):

Summary:

People with Parkinson's disease often experience a variety of nonmotor symptoms, the biological bases of which remain poorly understood. Johansson et al began to study potential roles of the dorsal raphe nucleus (DRN) degeneration in the pathophysiology of neuropsychiatric symptoms in PD.

Strengths:

Boi et al validated a transgenic reporter mouse line that can reliably label dopaminergic neurons in the DRN. This brain region shows severe neurodegeneration and has been proposed to contribute to the manifestation of neuropsychiatric symptoms in PD. Using this mouse line (and others), Boi and colleagues characterized electrophysiological and morphological phenotypes of dopaminergic and serotoninergic neurons in the raphe nucleus. This study involved very careful topographical registration of recorded neurons to brain slices for post hoc immunohistochemical validation of cell identity, making it an elegant and thorough piece of work.

In relevance to PD pathophysiology, the authors evaluated the physiological and morphological changes of DRN serotoninergic and dopaminergic neurons after a partial loss of nigrostriatal dopamine neurons, which serves as a mouse model of early parkinsonian

pathology. Moreover, the authors identified a series of physiological and morphological changes of subtypes of DRN neurons that depend on nigral dopaminergic neurodegeneration, LC noradrenergic neurodegeneration, or both. Indeed this works highlights the importance of LC noradrenergic degeneration in PD pathophysiology.

Overall, this is a well-designed study with high significance to the Parkinson's research field.

https://doi.org/10.7554/eLife.90278.2.sa2

Reviewer #2 (Public Review):

In this paper, Boi et al. thoroughly classified the electrophysiological and morphological characteristics of serotonergic and dopaminergic neurons in the DRN and examined the alterations of these neurons in the 6-OHDA-induced mouse PD model. Using whole-cell patch clamp recording, they found that 5-HT and dopamine (DA) neurons in the DRN are electrophysiologically well-distinguished from each other. In addition, they characterized distinct morphological features of 5-HT and DA neurons in the DRN. Notably, these specific features of 5-HT and DA neurons in the DRN exhibited different changes in the 6-OHDA-induced PD model. Then the authors utilized desipramine (DMI) to separate the effects of nigrostriatal DA depletion and noradrenalin (NA) depletion which are induced by 6-OHDA. Interestingly, protection from NA depletion by DMI pretreatment reversed the changes in 5-HT neurons, while having a minor impact on the changes in DA neurons in the DRN. These data indicate that the role of NA lesion in the altered properties of DRN 5-HT neurons by 6-OHDA is more critical than the one of DA lesion.

Overall, this study provides foundational data on the 5-HT and DA neurons in the DRN and their potential involvement in PD symptoms. Given the defects of the DRN in PD, this paper may offer insights into the cellular mechanisms that may underlie non-motor symptoms associated with PD. Despite the importance of the primary claim proposed by the authors, however, the interpretation of the authors on some DMI experiments is not explained well.

https://doi.org/10.7554/eLife.90278.2.sa1

Reviewer #3 (Public Review):

Summary:

Using ex vivo electrophysiology and morphological analysis, Boi et al. investigate the electrophysiological and morphological properties of serotonergic and dopaminergic subpopulations in the dorsal raphe nucleus (DRN). They performed labor-intensive and rigorous electrophysiology with posthoc immunohistochemistry and neuronal reconstruction to delineate the two major cell classes in the DRN: DRN-DA and DRN-5HT, named according to their primary neurotransmitter machinery. They find that the dopaminergic (DRN-DA) and serotonergic (DRN-5HT) neurons are electrophysiologically and morphologically distinct, and are altered following striatal injection of the toxin 6-OHDA. However, these alterations were largely prevented in DRN-5HT neurons by pre-treatment with desipramine. These findings suggest an important interplay between catecholaminergic systems in healthy and parkinsonian conditions, as well as a relationship between neuronal structure and function.

Strengths:

Large, well-validated dataset that will be a resource for others.
Complementary electrophysiological and anatomical characterizations.
Conclusions are justified by the data.

Relevant for basic scientists interested in DRN cell types and physiology
Relevant for those interested in serotonin and/or DRN neurons in Parkinson's Disease

Weaknesses:

Given the scope of the author's questions and hypotheses, I did not identify any major weaknesses.

https://doi.org/10.7554/eLife.90278.2.sa0

Author Response

The following is the authors' response to the original reviews.

> ***Reviewer #1 (Recommendations For The Authors):***
>
> *This manuscript aims to understand the biological mechanisms underlying neuropsychiatric symptoms in Parkinson's disease by characterizing subtypes of neurons in the dorsal raphe nucleus and defining their susceptibility to the degeneration of dopaminergic and adrenergic systems in the brain. This study was well-designed, the results were presented beautifully, and the manuscript was well-written. Here are some comments that may help to improve the overall quality of this work.*

We thank the reviewer for the kind comments.

> *Major concerns:*
>
> *The current study utilized an intrastriatal 6-OHDA injection, which raises the possibility that the observed electrophysiological and morphological changes of DRN5-HT and DRNDA neurons (Figs 3-6) may be due to the direct effects of 6-OHDA to DRN5-HT and DRNDA neurons projecting to the dorsal striatum (at least for DRN5-HT neurons). This possibility requires further clarification and discussion.*

6-OHDA is a catecholamine neurotoxin with low selectivity for serotonin neurons. However, changes in the levels of serotonin have been observed with high doses of 6OHDA. In our study, we used lower concentrations of 6-OHDA, which did not affect the levels of serotonin (Suppl. Fig 4D), or the number of DRN5-HT neurons (Suppl. Fig. 5B). Concerning the possible effect of 6-OHDA on DRNDA neurons, we did not observe any modification in the number of these cells in response to the administration of 6-OHDA (Suppl. Fig. 5C), (lines 170-175).

> *How does the loss of nigrostriatal dopamine neurons affect the electrophysiology and morphology of DRNDA neurons (Figs. 5-6)? What are the potential circuit mechanisms?*

The dopaminergic system in the midbrain and the DRN constitute two highly interconnected nuclei and hence there are multiple possible circuit mechanisms that could explain how loss of nigrostriatal dopaminergic neurons affects DRNDA neurons: First, DRNDA neurons are directly innervated by dopaminergic neurons in the SNc and VTA and hence loss of SNc inputs might evoke acute as well as homeostatic changes in DRNDA (Lin et al., 2020; Pinto et al., 2019). Second, midbrain dopaminergic neurons are in turn innervated by the DRN (Watabe-Uchida et al., 2012) and loss of postsynaptic dopaminergic neurons might affect all neuron types in the DRN that target the midbrain. Finally, GABAergic populations in the midbrain have been shown to target DRN5-HT neurons and might potentially also target other local cell types such as DRNDA (Li et al., 2019). Another possible pathway is the bidirectional connection between the striatum and the DRN (Pollak-Dorocic et al, 2014). DA

depletion in the striatum may affect the GABAergic projection to the DRN and in turn modify the properties of postsynaptic DRN neurons.

The potential circuit mechanisms are now included in the introduction (lines 58-59).

> *Whether these intrastriatal 6-OHDA mice exhibited nonmotor deficits (e.g., anxiety) that may be related to the observed changes in the DRN? Such behavioral data would enhance the overall conclusions of this work.*

The PD model utilized in this study displays non-motor deficits, including depression- and anxiety-like behavior (Masini et al. 2021, Ztaou et al., 2018). This is now highlighted in the manuscript (lines 167-169).

> *Minor issues:*
>
> *The panels of Fig. 2 should be re-labelled to match the descriptions in the main text (L. 142-158).*

Fig.2 now matches the descriptions in the main text.

> *Fig 4D was missing from the figure, which does not match the descriptions in the main text (L. 193-204:)*

Fig. 4D includes the parameters describing the dendritic branching and starts with the last graph on the right in the second row of the panel.

> *Line 409: Extra "as" after "average"*

Corrected in revised manuscript.

> *Fig 3G: Missed asterisks.*

Corrected in revised manuscript (Fig. 3G)

> *Details of how action parameters were quantified should be stated and specified in the methods.*

We have now added a section called ‘Quantification of electrophysiological parameters’ in the methods where we explain how the electrophysiological properties are defined and quantified (lines 407-439).

> *"Parkinson's disease" in the title should be revised to "parkinsonism"*

Corrected in revised manuscript.

> ***Reviewer #2 (Recommendations For The Authors):***
>
> *(1) Throughout the paper, there are numerous inaccuracies and inconsistencies in the figures, which impede the clear understanding of this paper. For example, there are discrepancies between the labeling of the main figures (sub-panels) and the corresponding manuscript (Figure 2, Figure 4).*

Corrected in the revised manuscript.

> *The statistical presentations are inaccurate in several figures (Figure 3E, 3G), making it difficult to distinguish which data is statistically meaningful. Furthermore, the number of cells presented in each figure is ambiguous in the figure legend. It would be better to avoid expressions such as 'n = 28 - 43 cells per group', as in line 456 (Figure 1I). Please provide the exact number of cells for each graph.*

We agree with the reviewer, and we have now added the precise n numbers for each panel in the corresponding legends in Fig 1, Fig 3, and Fig 5. Please note that some analysis was restricted to recordings where neurons fired close to their average spontaneous firing frequency (e.g. 1Hz for DRN5-HT) to allow for a fair comparison of the data across groups and that therefore the n numbers vary in different panels.

> *In some figures, the value of n in the graph seems different from the value of n in the figure legends (Figure 2G-I, Figure 4, Figure 6). Collectively, these inaccurate figures and the manuscript weaken the general credibility of the data presented.*

We apologize for the misunderstanding, but in the type of chosen graph, equal values are overlapped. The numbers described in the figure legend are correct.

> *(2) Some of the authors' claims in this paper are not supported by quantitative analysis, but only by sample recording traces or simple descriptions. For example, in line 97, the authors mentioned, "no differences when comparing TH-positive to TH-negative neurons".*
>
> *But there are no data actually analyzing these two groups in Supplementary Figure 2A.*
>
> *In addition, in line 103, there is a claim that "DRN DA neurons showed that they share several properties characteristics of other DA populations located in the SNc and the ventral tegmental area". However, this claim is backed up only by a few sample traces in Figure 1E.*
>
> *The statement (lines 110-111), "a relative constant action potential (AP) amplitude", is also not supported by appropriate quantitative analysis but only by sample recording traces.*

In our study we found a small subset of DAT-tdTomato positive neurons which did not stain positive for TH after the slice recordings. In 5 of 6 of these neurons (recorded in sham), the electrophysiological properties did not differ from other TH-positive neurons. This is visualized in Suppl. Fig 2A. The absence of any statistical difference was also confirmed by a Mann Whiteny U test comparing the TH negative to the TH positive DRNDA neurons (no significant differences in all 6 of 6 properties shown in Suppl. Fig 2A). Additionally, all these cells were DAT-positive, further supporting their classification as dopaminergic neurons. Therefore, we suspect that the lack of TH staining is likely caused by the tissue processing itself. Please note that all our immunohistochemistry was run on slices after several hours of patch-clamping procedures. Finally, including or excluding this small subset of neurons in the present study does not change any of the results presented and data was therefore pooled. We have now clarified this in more detail in the results section and in Suppl. Fig 2A (lines 100-103).

We have moved the comparison of hallmark properties found in DRNDA neurons as well as in dopaminergic neurons in the midbrain from the results section to the discussion (lines 281-283).

The claim that DRN5HT neurons have a comparatively constant action potential amplitude compared to DRNDA neurons is supported by quantitative analysis shown in Fig 1I (left

panel, “AP drop rate”), while the representative example traces are shown in Fig 1G.

> *(3) In the legend of Figure 2, the mouse used in this experiment is mentioned with two different names (wild-type mice in line 463 and sham-lesion mice in line 465). Is this a mistake? Or did the authors intentionally use the brain samples from sham-lesion mice for Figure 2?*

Figure 2 shows data in control conditions (Sham-lesion in our case), both from wild-type and Dat-Tomato. The text has been changed to avoid misunderstandings.

> *(4) While the primary claim of this paper is the differential alterations of DRN 5-HT and DA neurons in a mouse PD model, the observed changes in the DRN neurons of the 'DA only lesion model' are comparatively minor to the 'DA and NA lesions model'. Therefore, it looks like NA depletion has a more critical role in the DRN neurons of 6OHDA-lesion mice than DA depletion. To understand the results of this paper better, it would be great if the authors can provide additional data from the 'NA only lesion model'.*

We agree with the reviewer, and we have now added a new set of experiments in which we selectively lesioned noradrenergic cells by injecting 6-OHDA unilaterally into the LC. The new data are presented in supplementary figure 6 in the revised manuscript. We find that selective lesioning of the NA system affects DRNDA and DRN5-HT neurons mildly, suggesting that the concomitant lesion of the DA and NA systems is particularly impactful (possibly because of interactions between these two systems).

> *(5) In Figure 3B and Figure 5B, only the 6-OHDA+DMI group shows significant differences from the sham group. This finding might be attributed to the effect of DMI itself, not to the nigrostriatal DA degeneration without NA degeneration. Thus, adding the 'DMI-only group' in all experiments will strengthen the conclusion of this paper.*

The effect of one acute administration of desipramine was temporally limited to the stereotactic intervention (line 373-375), which was performed several weeks before the electrophysiological and morphological analyses. Given that the half-life of desipramine is approximately 24 hrs (Nagy and Johansson, 1975), we believe that its impact was limited to the neuroprotection of NA-neurons from 6-OHDA toxicity.

> *(6) DRN 5-HT neurons are known to exhibit cellular heterogeneity, and in particular their electrophysiological properties are quite heterogeneous (Bernat Kocsis. 2006; J.V. Schweimer. et al. 2011). Furthermore, 5-HT neurons in the distinct subregions of the DRN display different membrane properties (LaTasha K. Crawford, 2010). Therefore, not all DRN 5-HT neurons can be regarded as electrophysiologically identical. Given that the molecular identity of all recorded cells was confirmed with neurobiotin in this paper, it would be better to show that recorded cells are not biased toward certain subregions of DRN.*
>
> *In addition, providing more comprehensive descriptions of the electrophysiological features used in PCA analysis would be beneficial in understanding the electrophysiological profiling of DRN neurons explained in this paper.*

Although several studies have revealed electrophysiological and molecular heterogeneity within the DRN5-HT population, we did not observe any significant differences within the DRN5-HT neurons recorded in this study. We compared the properties of DRN5HT neurons recorded more anterior to those recorded in the posterior

DRN as well as neurons found in more ventral locations to those in more dorsal locations (data not shown). We would like to point out that the largest differences within serotonergic

neuron populations described by previous studies were often found when comparing those located in the medial raphe nucleus (MRN) to those found in the DRN. Calizo et al., (2011) showed for example significant differences in the input resistance and AHP amplitude between MRN5HT and DRN5HT neurons. These two properties as well as the AP amplitude, AP threshold, AP duration, and tau did however not differ between DRN subregions in their study - and neither in ours. We extended our Suppl. Fig 1 and mapped the location of DRN5HT and DRNDA neurons recorded in sham (Suppl. Fig 1D).

Overall, we've sampled neurons along the anterior-posterior and dorsal-ventral axes of the DRN, while on the medial-lateral axis, recorded DRN neurons were located medially.

We agree with the reviewer that a comprehensive description of the electrophysiological features was missing in the manuscript, and we have therefore added a new section in the materials and methods where we explain in detail how each parameter was measured and analyzed ('Quantification of electrophysiological parameters', lines 407-439). This section also provides detailed information about the five properties underlying the PCA shown in figure 1 (i.e. delay to the first action potential, action potential drop rate, action potential rise time, duration of the afterhyperpolarization, and capacitance).

> *(7) Some sample images presented in this paper contain information that can conflict with the previous research. In Figures 4B and 6B, TH expression was significantly increased in the DMI pretreatment group compared to the control group. However, several studies have shown that the administration of DMI decreases TH expression levels (Komori et al.1992; Nestler et al.1990). Therefore, it would be great if the authors further explained how the pretreatment of DMI with 6-OHDA affects TH level within the DRN.*

Figure 4B and 6B do not show any quantification of TH expression. The difference observed in the representative pictures is casual and due to the variable expression of TH across the slice. Moreover, as mentioned in the response to point 5, mice were subjected to a single injection of DMI immediately preceding the stereotactic intervention (line 373375). In contrast, the increase in TH expression reported by Komori et al. 1992 and Nestler et al. 1990 was observed in response to chronic (two weeks) administration of DMI.

> *(8) This paper lacks direct evidence to demonstrate whether DMI pretreatment could effectively protect against NA depletion. Therefore, in addition to TH expression levels, it is important to provide data to confirm the intact NA levels (or NA axons) after DMI treatment.*

NA levels in the striatum were measured by Enzyme-linked immunosorbent assay and reported in Suppl.Fig.4 in the revised manuscript.

> *(9) It would be great if the authors specifically explained why 6-OHDA was injected into the striatum (neither MFB nor SNc) to make a mouse model of PD.*

Mice were injected in the dorsal striatum to produce a partial bilateral lesion of the dopamine and noradrenaline systems. This model reproduces the initial stages of PD and also recapitulates several non-motor symptoms of PD, including affective disorders, which may be related to changes in serotonergic and dopaminergic transmission in the dorsal raphe. In contrast, injections in the MFB and SNc quickly produce a severe motor phenotype closer to a late stage of the disease and cannot be done bilaterally.
The striatal model has been successfully used in other publications (Kravitz et al., 2010, Masini et al., 2021, Ztaou et al., 2018, Chen et al., 2014, Branchi et al., 2008, Marques et al. 2019, Tadaiesky et al., 2008, Matheus et al., 2016, Silva et al., 2016).

> *(10) Supplementary Figures 2 and 3 were erroneously cut on the right side. These figure images should be replaced with the correct ones.*

We thank the reviewer for noticing and we have now replaced the figures with the correct ones.

> *(11) There should be more explanations about tdTomato-positive but non-TH neurons in Supplementary Figure 2. It is strange to regard TH-negative neurons as DA neurons although these neurons have DA neuron-like electrophysiological properties. If these tdTomato-positive but non-TH neurons cannot release DA, can we say these are DA neurons?*

In our study we found a small subset of DAT-tdTomato positive neurons which did not stain positive for TH afterwards. In 5 of 6 of these neurons (recorded in sham), the electrophysiological properties did not differ from other TH-positive neurons. This is visualized in Suppl. Fig 2A. The absence of any statistical difference was also confirmed by a Mann Whiteny U test comparing the TH-negative to the TH-positive DRNDA neurons (no significant differences in all 6 of 6 properties shown in SF2A). Additionally, all these cells were DAT-positive, further supporting their classification as dopaminergic neurons. Therefore, we suspect that the lack of TH staining is likely caused by the tissue processing itself. Please note that all our immunohistochemistry was run on slices after several hours of patch-clamping procedures. Finally, including or excluding this small subset of neurons in the present study does not change any of the results presented and data was therefore pooled. We have now clarified this in more detail in the results section and in Suppl. Fig 2A (lines 100-103).

> ***Reviewer #3 (Recommendations For The Authors):***
>
> *The authors report using a parametric statistical test, the t-test. The t-test makes the assumption that the data are normally distributed. Most biological data is not distributed normally, and with smaller datasets, it is difficult to say whether the underlying distribution would be normally distributed. I would recommend using the non-parametric versions of the same test (eg Mann-Whitney U test), which is likely to give a similar result while being more conservative given the potential for non-normal distribution.*

All electrophysiological data were first tested for normality before running the corresponding statistical test (either t-test for normal distributed data or Mann-Whitney U test for non-normally distributed data). The morphological data are now analyzed by the Mann-Whitney U test (lines 484-494).

> *The authors state that mice were treated with 6-OHDA at 3 months, then brain slices were prepared 3 weeks later, making them about 4 months old. I could not find the age of sham/control mice and 6-OHDA/desipramine mice in the methods section. Were sham/controls and 6-OHDA slices prepared in an interleaved fashion?*

Sham and 6-OHDA+DMI mice underwent surgery at 3 months and the brain slices were prepared 3 weeks later, as the 6-OHDA mice. We have now clarified this in the methods (line 381).

> *While desipramine is relatively selective as a norepinephrine reuptake inhibitor, it also can prevent serotonin reuptake. Could this mechanism also protect DRN neurons from the effects of 6-OHDA?*

Even if desipramine has some affinity for the serotonin reuptake, this affinity is 100-fold less than the one described for the noradrenaline reuptake (Richelson and Pfenning, 1984, Gillman, 2007). Moreover, in our study the 6-OHDA injection in the dorsal striatum did not cause any direct damage to the DRN5-HT, as shown by the 5-HT measurement and DRN5-HT counting (Suppl. Fig. 4D, Suppl. Fig. 5A,B), so we can exclude that the effects observed in the DMI+6-OHDA group are related to a protection of the serotonergic system exerted by a single injection of desipramine.

> *On line 168, the authors use the abbreviation NA for noradrenergic. Was this abbreviation previously defined in the manuscript?*

Yes, the abbreviation is defined in the introduction (line 73).

> *On line 45, the authors cite that the DRN-5HT subpopulation accounts for 30-50% of the DRN neurons. It would be helpful to know approximately what percentage of the DRN neurons belong to the DRNDA subpopulation as well.*

To the best of our knowledge, there is unfortunately no detailed analysis of the prevalence of DRNDA neurons in mice available. Previous studies in rats have estimated that this population comprises around 1000 neurons (Descarries et al., 1986). According to Calizo et al. (2011), the number of any non-serotonergic neuron population (releasing dopamine or other neurotransmitters) in the DRN is one third to one tenth less than the number of DRN5-HT neurons. But please note that this study was also performed in rats (line 55).

> *While I appreciate that the authors did not over-interpret their findings, it would be useful to comment (in the Discussion) on how their findings could/should be used in interpreting other studies using 6-OHDA, as well as the relationship of their findings to loss of 5-HT and/or DRN neurons in Parkinson's Disease itself.*

In the manuscript, we refer to the utility of the 6-OHDA model for the study of a wide range of non-motor symptoms. We have now described, in this model, how the loss of midbrain dopaminergic and noradrenergic neurons affects the electrophysiological and morphological properties of DRN5-HT and DRNDA neurons. This information will allow for a more precise assessment of the mechanisms involved in the affective and cognitive aspects of PD symptomatology (lines 354-356).